AD-A052 638 MASSACHUSETTS INST OF TECH CAMBRIDGE DEPT OF ELECTRI--ETC F/G 20/4
FIRST-QUADRANT TWO-PHASE FLOW IN CENTRIFUGAL PUMPS.(U)
JAN 77 R D ZEGLEY

UNCLASSIFIED NL

1 OF 2
AD A052638

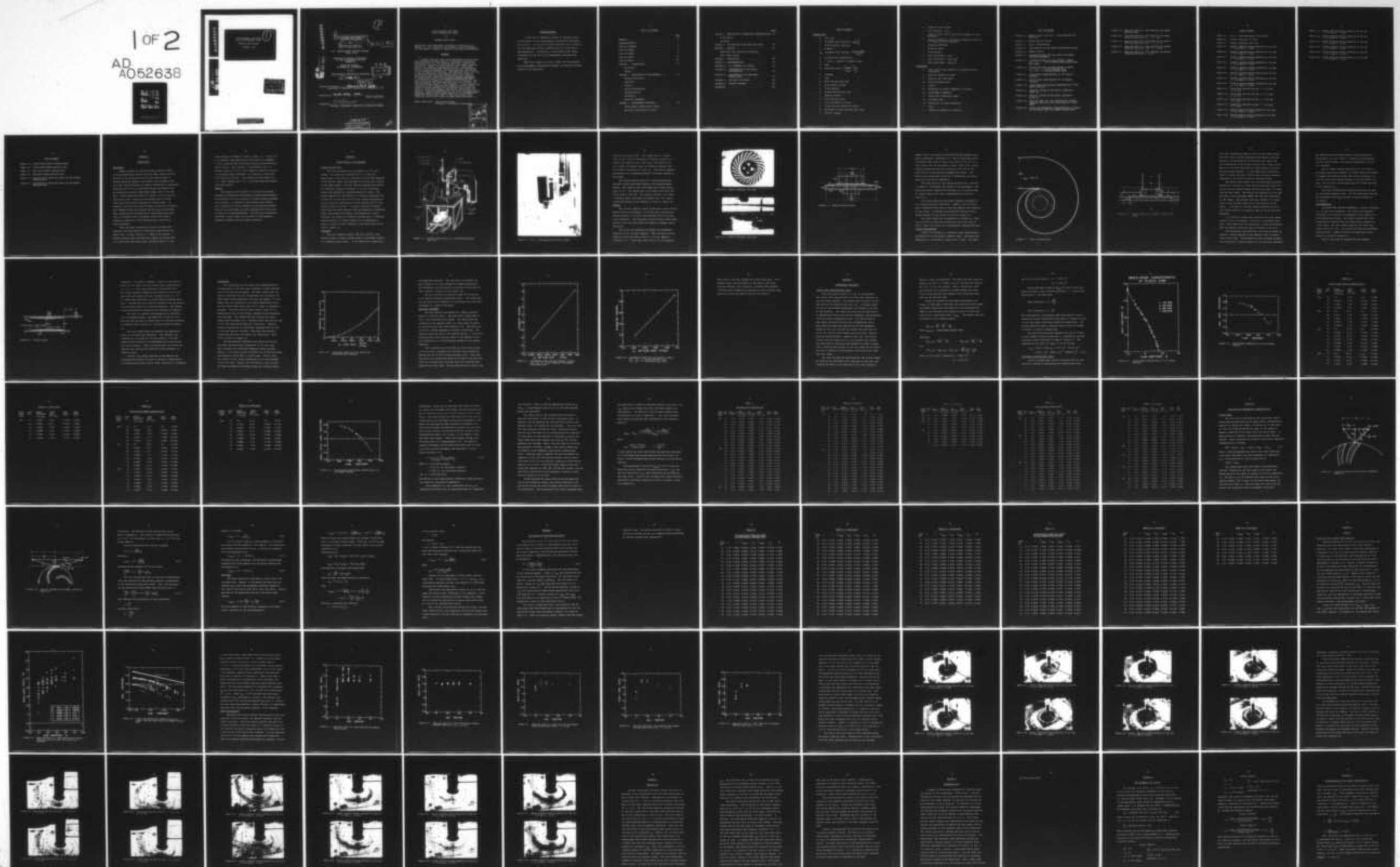

AD A052638

1
2

FIRST-QUADRANT TWO-PHASE FLOW IN CENTRIFUGAL PUMPS

RAYMOND DAVID ZEGLEY

JANUARY, 1977

DDC FILE COPY

DDC
RECEIVED
APR 4 1978
F

This document has been approved for public release and sale; its distribution is unlimited.

AD A052638
AD No.
DDC FILE COPY

(1)

(6)

FIRST-QUADRANT TWO-PHASE FLOW IN CENTRIFUGAL PUMPS.

by

(10) RAYMOND DAVID ZEGLEY

(9) Master's thesis

B.S., UNITED STATES MILITARY ACADEMY
(June, 1973)

SUBMITTED IN PARTIAL FULFILLMENT
OF THE REQUIREMENTS FOR THE
DEGREE OF

MASTER OF SCIENCE
IN MECHANICAL ENGINEERING

at the

MASSACHUSETTS INSTITUTE OF TECHNOLOGY

(11) Jan[redacted], 1977

DDC
RECEIVED
APR 4 1978
F

(12) 109p.

Signature of Author.......Raymond David Zegley.......
Department of Mechanical Engineering, January 21, 1977

Certified by David Gordon Wilson..............................
Thesis Supervisor

Accepted by W M Rohsenow..............................
Chairman, Department Committee on Graduate Students

220 015.

This document has been approved for public release and sale; its distribution is unlimited.

JB

FIRST-QUADRANT TWO-PHASE
FLOW IN CENTRIFUGAL PUMPS

by

RAYMOND DAVID ZEGLEY

Submitted to the Department of Mechanical Engineering on January 21, 1977 in partial fulfillment of the requirements for the degree of Master of Science in Mechanical Engineering.

ABSTRACT

A pump system was built and instrumented on which tests were performed yielding single- and two-phase actual pump characteristics for first-quadrant operation (forward flow and forward rotation) of two different centrifugal impellers mounted in a simple two-dimensional volute. Theoretical single- and two-phase pump characteristics were determined from the impeller geometry, the Euler equation, and the use of the two-phase flow function. The head-loss ratio, the loss of head in two-phase flow divided by the loss of head in single-phase flow, was then plotted versus void fraction. The results were compared to an earlier theory proposed by J. Mikielewicz and D. G. Wilson which predicted the head-loss ratio to be primarily a function of void fraction. ~~My~~ These results indicate that the head-loss ratio is a function of flow coefficient as well as void fraction. Flow-visualization studies were also conducted and revealed that flow regime inside the blade passages can be different from either the inlet or outlet flow regimes, and greatly affects pump performance. Further experimentation, on a more efficient system employing higher-specific-speed impellers, is recommended to study more closely the effect of flow coefficient, flow regime and void fraction upon two-phase pump performance.

Thesis supervisor: David Gordon Wilson
professor of mechanical engineering

ACCESSION for
NTIS White Section
DDC Buff Section
UNANNOUNCED
JUSTIFICATION Per ltr on file
BY
DISTRIBUTION/AVAILABILITY CODES
Dist. SPECIAL
A

ACKNOWLEDGEMENTS

I would like to express my thanks to Professor David Gordon Wilson for his encouragement and guidance throughout this project. I also wish to thank Professor Peter Griffith, Mr. Tak-chee Chan, and Mr. Charles Snell for their advice and suggestions. In addition, I am grateful to Mr. Randy Coverstone for the use of his photographic equipment and expertise.

Above all, thanks to my wife, Linda, for her patience and encouragement throughout my studies, and for her accurate typing of the manuscript.

TABLE OF CONTENTS

LIST OF SYMBOLS

NOMENCLATURE

A	flow area
a	two-phase flow function $\equiv (\frac{\alpha}{1-\alpha})\frac{\rho_V}{\rho_L}$
C	fluid velocity, absolute
d	diameter
f_{tp}	two-phase flow function $\equiv \frac{(1+a)(1+as^2)}{(1+as)^2}$
g	gravitational acceleration
g_c	$\equiv$ (ma/F) $\equiv$ constant in Newton's Law
H	head
H^*	head-loss ratio $\equiv \frac{\psi'_{tpth} - \psi'_{tp}}{\psi'_{spth} - \psi'_{sp}}$
h	enthalpy
m	mass
$\dot{m}$	mass flow per unit time
N	rotor speed, rev/min
p	fluid pressure
Q	volume flow per unit time
r	impeller radius
s	slip velocity ratio
u	rotor peripheral velocity
W	fluid velocity relative to rotor
$\dot{W}$	work done by pump rotor per unit time
x	quality $\equiv \dot{m}_V/\dot{m}_T$

Z number of rotor blades

α void fraction $\equiv A_V/A_T$

β angle of fluid vector relative to tangent to rotor periphery

β' angle of tangent to rotor-blade centerline relative to tangent to rotor periphery

Δ property difference

δ deviation angle

ρ fluid density

ϕ flow coefficient $\equiv C_m/u$

ψ work coefficient $\equiv g_c \Delta h_o/u_2{}^2$

ψ' head coefficient $\equiv g\Delta H_o/u_2{}^2$

SUBSCRIPTS

o total (static plus dynamic) or stagnation value of property

1 plane at entrance to rotor

2 plane at exit from rotor

be best-efficiency point

L liquid

m meridional or radial component of velocity

sp single-phase component

T total flow, liquid plus vapor

tp two-phase flow

th theoretical or ideal conditions

v vapor

θ tangential component of velocity

LIST OF FIGURES

LIST OF PHOTOS

PHOTO 6-15: BRONZE IMPELLER DURING OPERATION AT 400 RPM, $\alpha = 0.10$ AND $\phi = 0.0738$

PHOTO 6-16: BRONZE IMPELLER DURING OPERATION AT 400 RPM, $\alpha = 0.20$ AND $\phi = 0.0799$

PHOTO 6-17: BRONZE IMPELLER DURING OPERATION AT 200 RPM, $\alpha = 0.30$ AND $\phi = 0.1131$

PHOTO 6-18: BRONZE IMPELLER DURING OPERATION AT 200 RPM, $\alpha = 0.40$ AND $\phi = 0.1230$

PHOTO 6-19: BRONZE IMPELLER DURING OPERATION AT 400 RPM, $\alpha = 0.30$ AND $\phi = 0.0565$

PHOTO 6-20: BRONZE IMPELLER DURING OPERATION AT 400 RPM, $\alpha = 0.40$ AND $\phi = 0.0615$

LIST OF TABLES

CHAPTER 1

INTRODUCTION

BACKGROUND

Safety analyses of loss-of-coolant accidents (LOCA) in pressurized-water nuclear reactors (PWR) require the prediction of the performance of the main-coolant pumps in several operating modes in both single- and two-phase flow. In a PWR, sub-cooled water at nominal conditions of (typically) 2250 psig and 577 F is circulated through the reactor core by several main-coolant centrifugal pumps, each in its own leg. A LOCA occurs when there is a *break in one or more of* the coolant legs, causing the sub-cooled water to flash into steam while flowing through the coolant pumps. In addition, the flow can either maintain or reverse its direction, depending upon the location and the size of the break. Thus, prediction of the behavior of centrifugal-pump operation in two-phase flow is necessary before the thermal-hydraulic response of a PWR system during a LOCA can be fully predicted.

There has been a continuing effort to predict more precisely the performance of centrifugal pumps during two-phase flow. In May of 1964 D. J. Olson of the Aerojet Nuclear Company (ANC) published the results of testing done on a half-scale centrifugal pump, which was part of a test

loop designed to simulate a LOCA in a PWR. G. L. Sozzi and G. W. Burnette published similar test results in November of 1971, obtained from the General Electric one-sixth-scale test facility. More recently, J. Mikielewicz and D. G. Wilson, working at M.I.T., have proposed a method of predicting two-phase pump performance as a function of head-loss ratio and void fraction. This method has been applied be T. C. Chan, studying at M.I.T., to the ANC data with reasonably good results.

PURPOSE

The purpose of this report is to refine the method proposed by Mikielewicz and Wilson by investigating whether the head-loss ratio is a function of other variables besides void fraction. In addition, flow-visualization studies were conducted to gain an insight into the physical phenomenon of the flow inside the blade passages and volute, and its effects on pump performance. The tests and conclusions contained in this report are confined to first-quadrant operation (forward flow and forward rotation).

CHAPTER 2

DESCRIPTION OF THE APPARATUS

GENERAL DESCRIPTION

The tests conducted were performed on an air-water system. City water at a pressure of 50 ± 5 psig was supplied by a 1.61-inch I.D. pipe while the air was supplied by the lab-air supply line through a 0.25-inch nylon fitting in the inlet piping. The test facility employed two different impellers, mounted vertically in a clear Plexiglass casing, and powered by a variable-speed A.C. motor. The casing emptied into the botoom of a 55-gallon drum which was fitted with a metal weir to allow for constant backpressure during operation, and having a 4-inch-diameter drain on the opposite side of the weir. A venturi was used to measure water-flow rate while the air flow was measured by rotameters. Static head across the impeller was measured by a water manometer and supply air pressure was measured by a standard pressure gauge. An overall diagram of the apparatus is given in figure 2-1 and a picture of the actual test rig is given in photo 2-1.

IMPELLERS

The first impeller used in the test rig was a low-specific-speed, low-head, molded-plastic centrifugal impeller with backward-swept blades. It had twenty-four blades and a

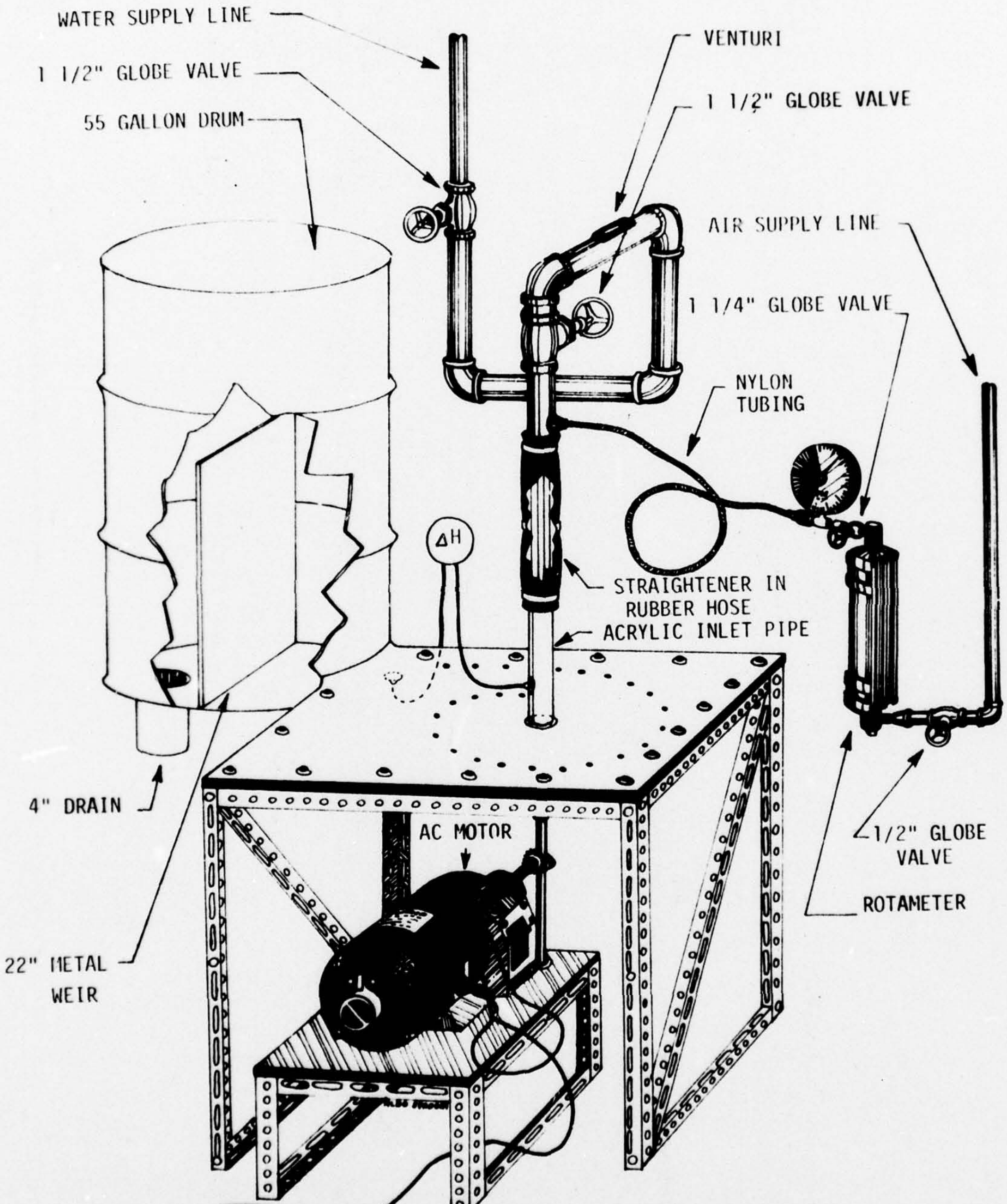

FIGURE 2-1. OVERALL VIEW OF THE M.I.T. FLOW-VISUALIZATION TEST LOOP

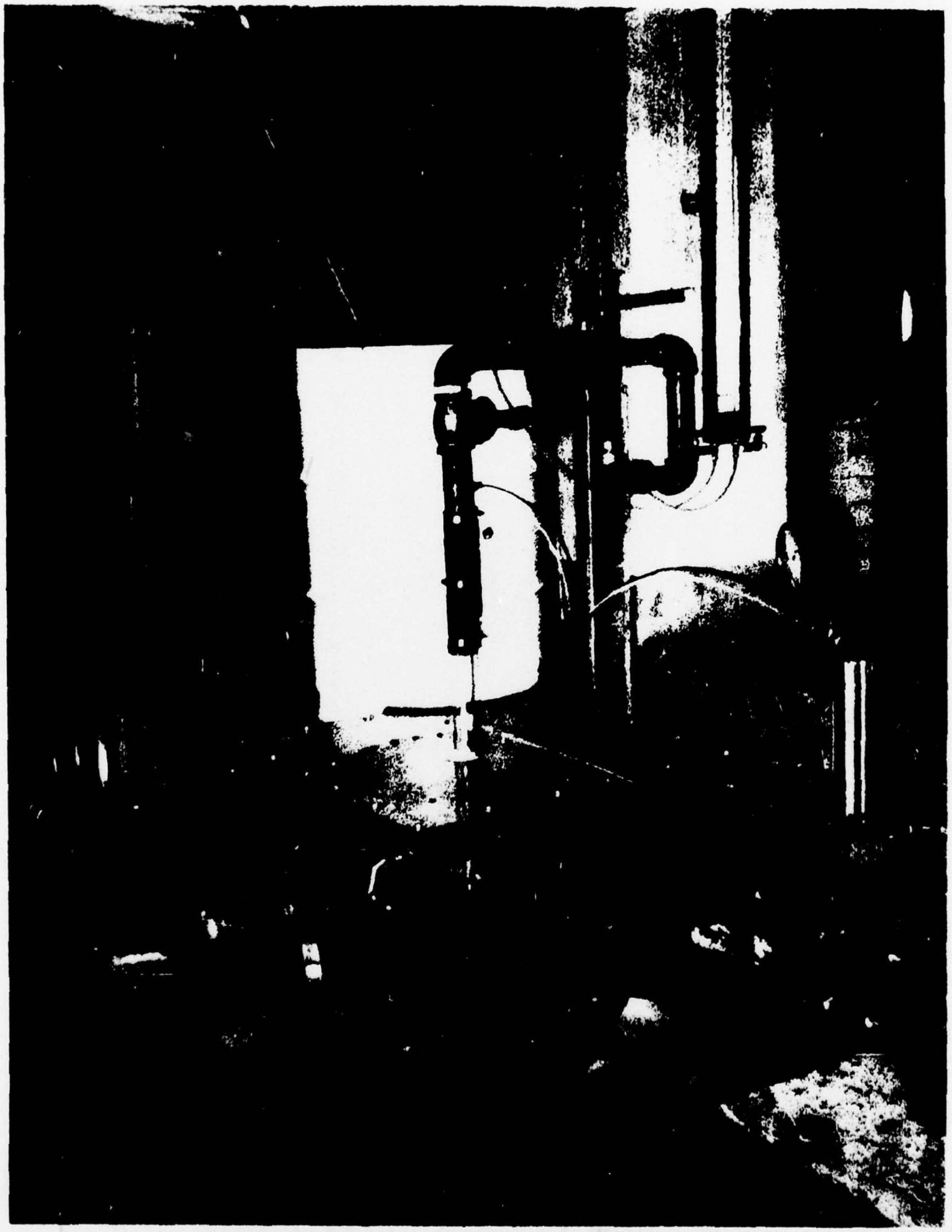

PHOTO 2-1. M.I.T. FLOW-VISUALIZATION TEST SYSTEM

blade outlet angle of 46°. The blades were 0.5 inches thick at the tips and maintained a constant height of 0.5 inches from shroud to tip. The eye of the impeller was 4.25 inches in diameter while the blade-tip diameter was 8.19 inches (see photos 2-2 and 2-3). The plastic impeller was mounted on an aluminum backplate to prevent warping at high speed.

The second impeller used was a low-specific-speed, shrouded, brass centrifugal impeller with backward-swept blades. This impeller had five blades and a blade outlet angle of 25°. The blades were 0.25 inches thick and 0.385 inches high at the tips. The impeller eye was 2.81 inches in diameter while the blade-tip diameter was 7.31 inches. A detailed drawing of the impeller is given in figure 2-2.

CASINGS

The original impeller casing consisted of three 30-inch square pieces of Plexiglass: a 0.5-inch thick scroll piece encased between a 0.5-inch thick backplate and a 0.25-inch thick coverplate. The Plexiglass casing allowed visual observation of the flow both within the impeller passages and in the scroll.

The scroll was designed for optimum first-quadrant operation of the original impeller. This was done by first assuming a best efficiency value of ϕ for the impeller (reference 2-1). Based upon this value of ϕ, the impeller

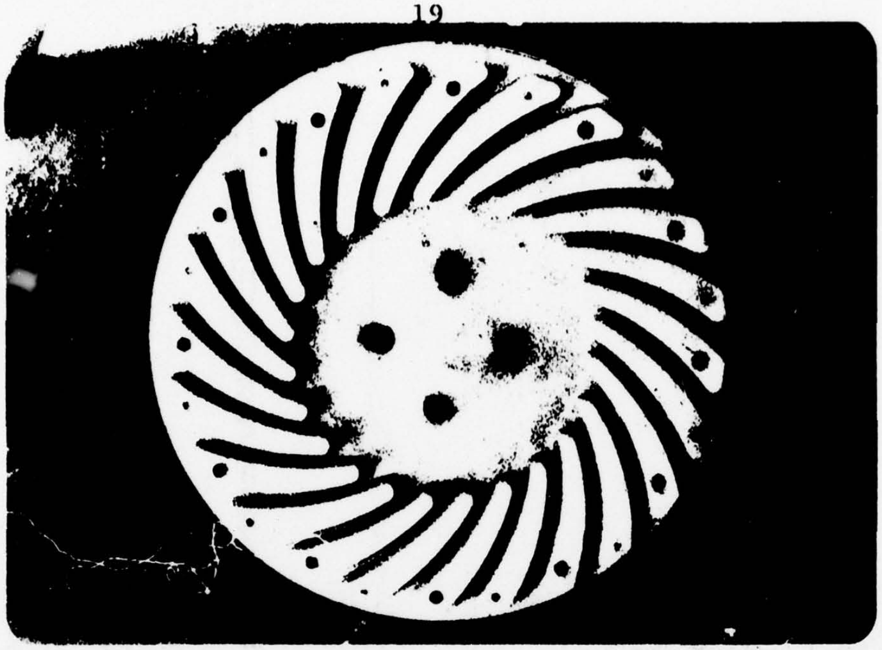

PHOTO 2-2. PLASTIC IMPELLER, TOP VIEW

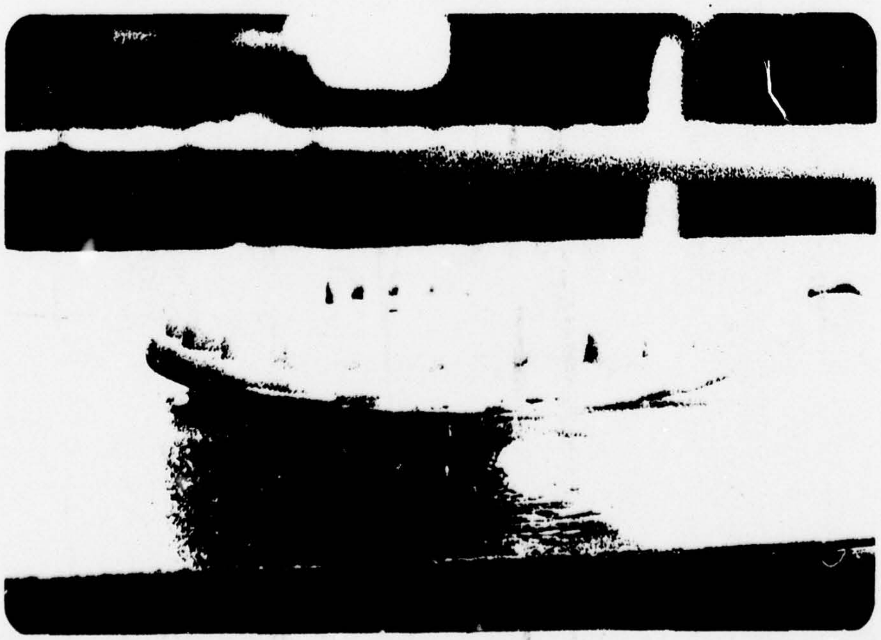

PHOTO 2-3. PLASTIC IMPELLER, SIDE VIEW

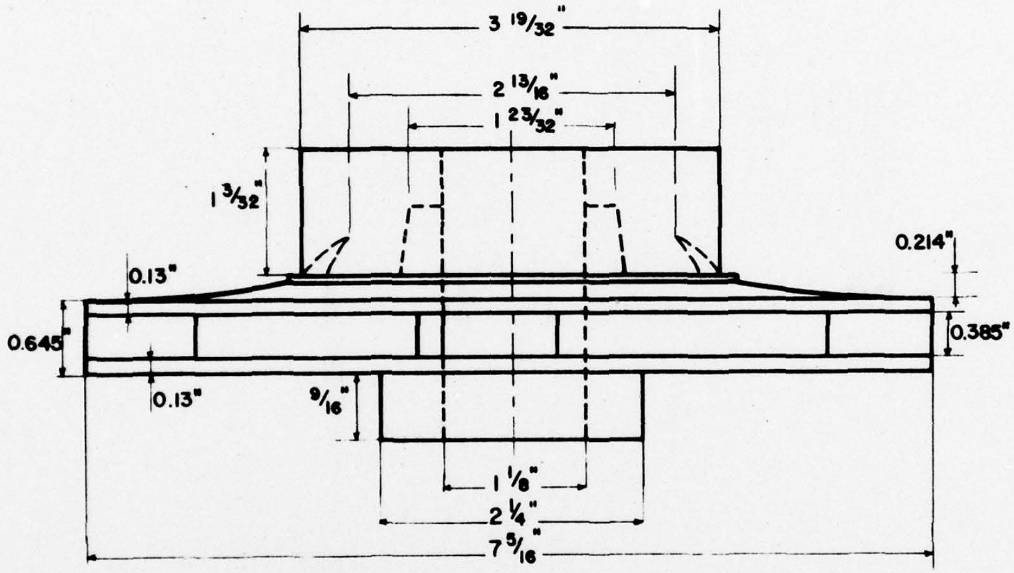

FIGURE 2-2. BRONZE-IMPELLER DESIGN

geometry and a slip-angle calculated from the Busemann slip-factor correlation (reference 2-2), the 0.5-inch deep scroll increased 0.388 inches in radius for every 15° of arc to a total outlet area of 4.66 square inches. This scroll configuration allowed the absolute velocity of the flow at the blade tips to be maintained throughout the scroll. The details and calculations involved in determining the scroll shape are contained in Appendix B.

The inlet piping to the casing consisted of a vertical 1.5-inch-I.D. Plexiglass tube joined to the coverplate. The casing and scroll emptied into the base of a 55-gallon drum. An overall view of the scroll configuration is given in figure 2-3.

The casing used with the second impeller consisted of the original backplate and scroll. However, two 0.75-inch thick coverplates were used to seal the impeller more securely in the casing. A detailed cross-sectional drawing of the second impeller in the casing is given in figure 2-4.

The inlet piping was increased to 2.5-inches-I.D. Plexiglass tubing to match more closely the eye of the new impeller, while the scroll exit configuration remained the same.

PIPING CONFIGURATION

Figure 2-1 and photo 2-1 show the overal system piping configuration for the plastic impeller tests. The water was supplied by a 1.61-inch-I.D. pipe at 50 ± 5 psig. The water

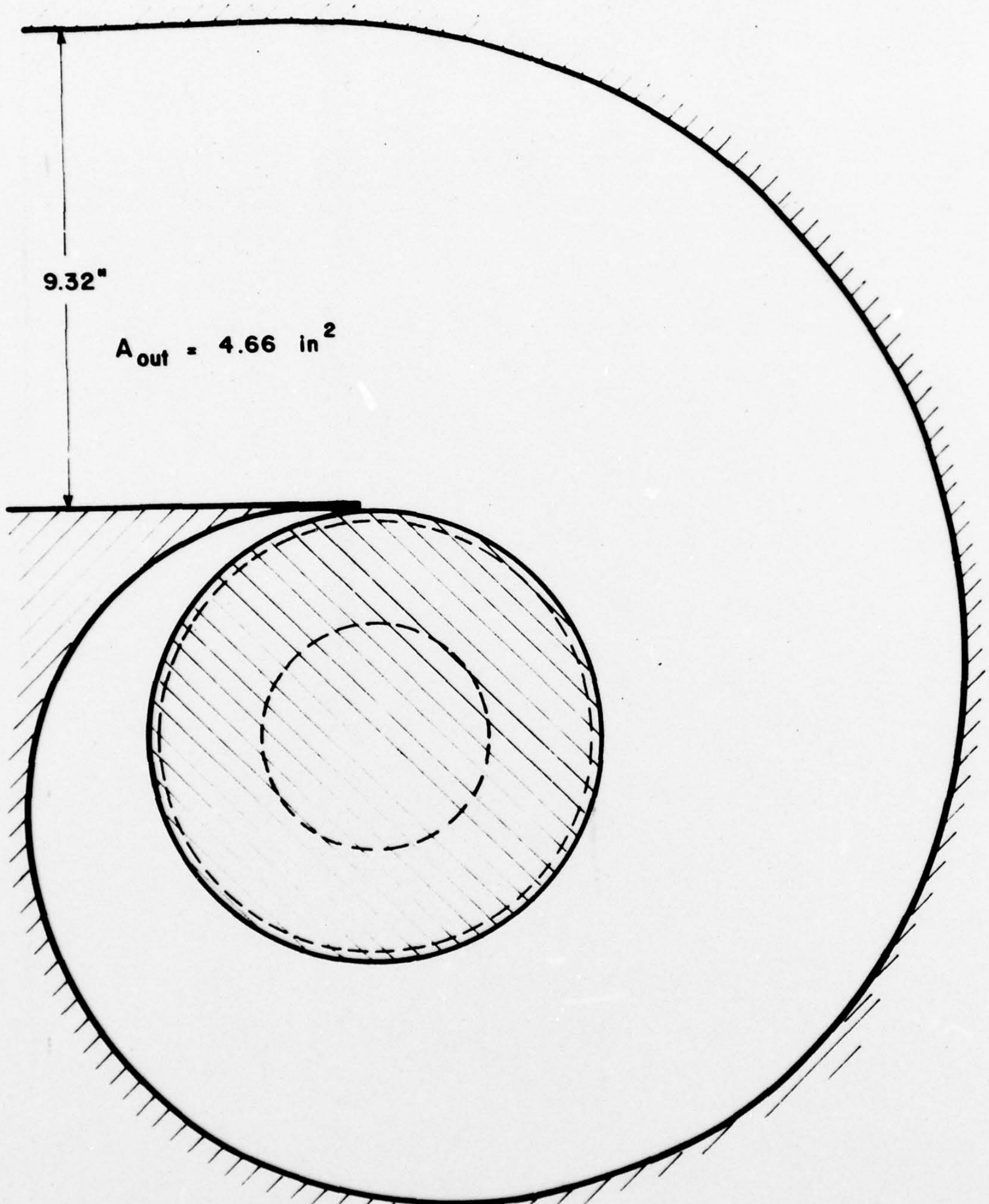

FIGURE 2-3. SCROLL CONFIGURATION

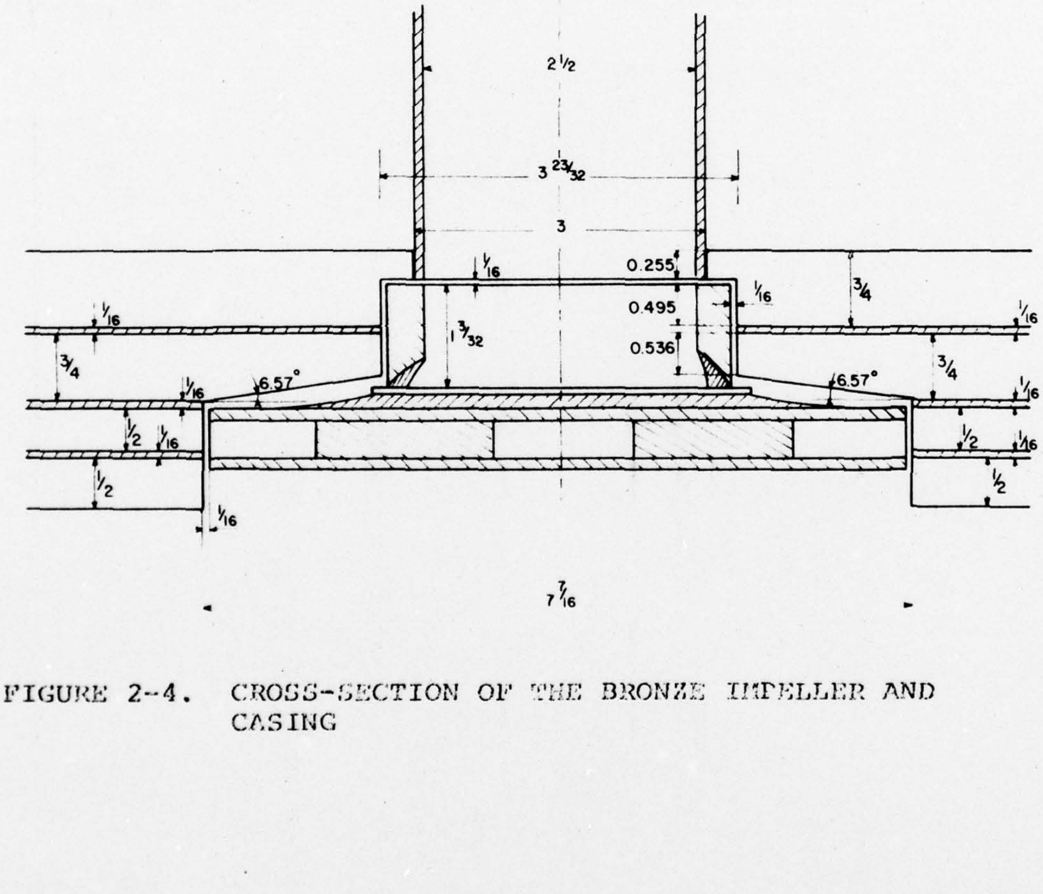

FIGURE 2-4. CROSS-SECTION OF THE BRONZE IMPELLER AND CASING

flow was controlled by means of two 1.5-inch globe valves. The first valve, located upstream of the venturi, was regulated to set the majority of the flow rates, while the valve downstream of the venturi remained fully open, except when very low water-flow rates of approximately 10 gallons per minute were desired. In such cases, both valves were used to regulate the water flow so that the water manometer connected to the venturi could be read more easily.

The venturi was located in a 16.5-inch-long horizontal section of 1.61-inch-I.D. pipe with the entrance plane 9.47 inches from the forward elbow, and the exit plane 2.7 inches from the rear elbow. The venturi was inserted into the pipe and held in place by epoxy cement and the valve connection at the throat. The pressure taps were located 3.25 inches ahead of the entrance plane and at the mid-point of the throat. 0.25-inch-O.D. Polyflo tubing connected the 1/4-inch globe vlaves at the pressure taps to the 60-inch water manometer.

A 12-inch-long rubber hose connected the steel supply piping to the 10-inch-high, 1.5-inch-I.D. Plexiglass inlet pipe. This rubber hose also contained a 5-inch straw-bundle flow straightener which was used to minimize inlet swirl.

The Plexiglass inlet pipe had a 1/32-inch pressure tap located 3 inches upstream of the impeller inlet to measure inlet static head. This pressure tap was connected by means of 0.25-inch-O.D. Polyflo tubing to a 30-inch water manometer.

The pump-outlet static-head pressure tap was located at mid-stream in the exit volute, 7 inches from the entrance to the 55-gallon drum, and similarly connected to the 30-inch manometer.

The air-supply system consisted of the 1/2-inch-I.D. air-supply pipe being reduced to 1/4-inch, being fed through a rotameter and pressure gauge, and finally injecting air into the inlet steel piping through a 1/8-inch Polyflo fitting. The air-inlet fitting was located 22 inches upstream of the impeller eye.

The piping configuration remained basically the same for the bronze impeller tests. The only alteration was that the Plexiglass inlet pipe now had an inside diameter of 2.5 inches.

INSTRUMENTATION

The water-flow rate was measured by a venturi connected to a 60-inch water manometer. The venturi was designed (reference 2-3) and built to accomodate a flow range of 10 to 70 gallons per minute. The throat diameter was 1.258 inches and the entrance and exit planes had a diameter of 1.544 inches. The inlet angle measured 5.52° while the outlet angle was 3.98°. The venturi was made from machined aluminum stock. Complete details and dimensions of the venturi are given in figure 2-5.

The air-flow rate was measured by two separate

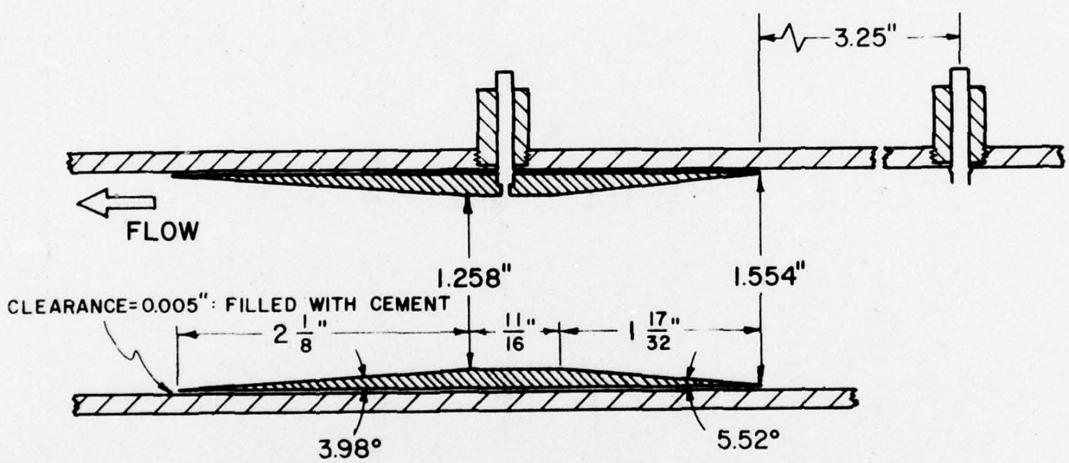

FIGURE 2-5. VENTURI DESIGN

rotameters, The smaller rotameter, used for flow rates of 0.002 to 0.014 cubic feet per second, was a Fischer-Porter 1/4 - 20 - G - 5/81 glass tube with a black-bead float. The larger rotameter covered a flow range of 0.02 to 0.10 cubic feet per second, and was a Fischer-Porter 1/2 - 27 - G - 10/80 glass tube with a 0.5-inch SVT-45 stainless-steel float. Through the use of the two rotameters and the venturi, void fractions from 0.0 to 0.62 were obtained. The details of the void-fraction calculation are discussed in Chapter 3.

The inlet air pressure was measured by an Acco Helicoid air-pressure gauge. The gauge had a range of 0.0 to 60.0 psig and was used to record inlet air pressure necessary to determine the slip-ratio, s, and the two-phase density, ρ_{tp}.

The static head across the impeller was measured by means of a 30-inch water manometer. This manometer was connected by 0.25-inch-O.D. Polyflo tubing to 1/32-inch pressure taps located in the Plexiglass inlet pipe and the exit scroll channel. Thus, the static-head rise across the impeller was read directly from the 30-inch manometer in inches of water.

Finally, the angular velocity of the impeller was determined by matching its rate of rotation, controlled by a variable-speed electric motor, with a setting on a Strobotac.

CALIBRATION

The calibration of the venturi was conducted while it was physically in the test loop, although a slight modification of the loop was necessary. The short rubber-hose connection containing the flow straightener and connecting the metal pipe to the Plexiglass inlet pipe was removed. A long rubber hose was connected to the piping immediately following the second globe valve, and led to a sump at atmospheric pressure. The water flow was then turned on and set to a steady-state value on the venturi manometer while exhausting into the sump. Once steady flow was achieved the large rubber hose was swung into a 55-gallon catch tank and the time to fill the drum was recorded by a stop watch. Numerous values of ΔH were set on the venturi manometer and the time to fill the drum was recorded. From these data points a calibration curve for the venturi was constructed. This curve is shown in figure 2-6.

The two separate rotameters used during the testing were also calibrated while physically in the test loop. Each rotameter was calibrated separately using the same method. A five-gallon plastic container was filled with water and submerged upside down in a water sump. The air flow was turned on and a steady reading was set on the rotameter in the test loop. Tubing, 0.25-inch Polyflo, was run from the test loop behind the pressure gauge and inserted inside

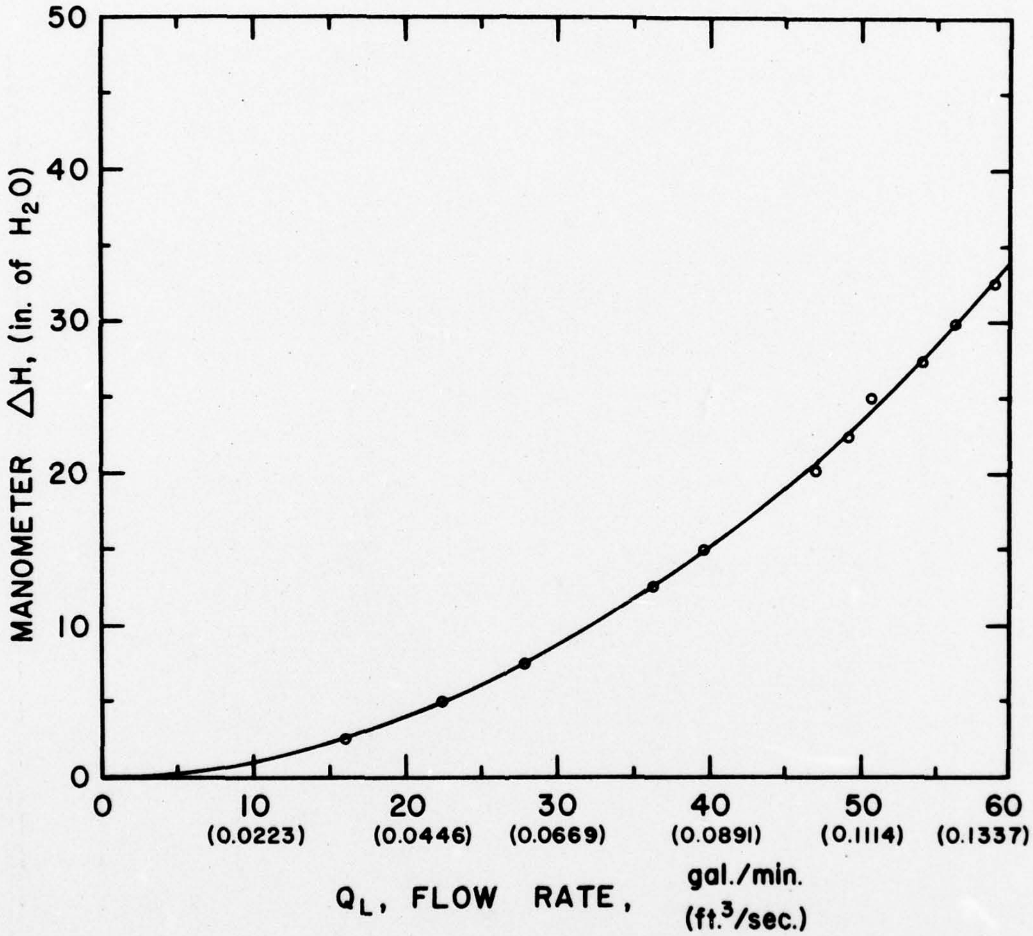

FIGURE 2-6. CALIBRATION CURVE FOR THE VENTURI AND WATER-FLOW-RATE MANOMETER

the submerged container. The time taken to displace the known volume of air was recorded for numerous settings on the rotameters, and calibration curves were constructed for both rotameters (figure 2-7 and figure 2-8).

The Acco Helicoid air-pressure gauge was calibrated on an Ashcroft portable dead-weight tester. The gauge reading was found to be constantly 0.5 psig below the true value throughout the range of the gauge.

AUXILIARY EQUIPMENT

The pump impeller was powered by a Master variable-speed A.C. electric motor. The motor had a speed range of 180 to 1725 revolutions per minute. The motor shaft was connected to the impeller shaft at a right angle by means of two bevel gears with tooth angles of 23°. The motor was bolted to a wooden baseplate to minimize vibrations. The impeller shaft was held at the impeller end by a 1 3/16-inch stainless-steel ball bearing, while at the opposite end it was connected to a 1/2-inch bearing attached to the wooden baseplate.

The 55-gallon drum into which the scroll emptied was used to provide a constant back pressure during operation, through the use of the 22-inch-high metal weir. Flow from the scroll exit entered the drum on one side of the weir and built up in height until spillage over and around the weir equalled the input flow. The spillage exited the drum on the

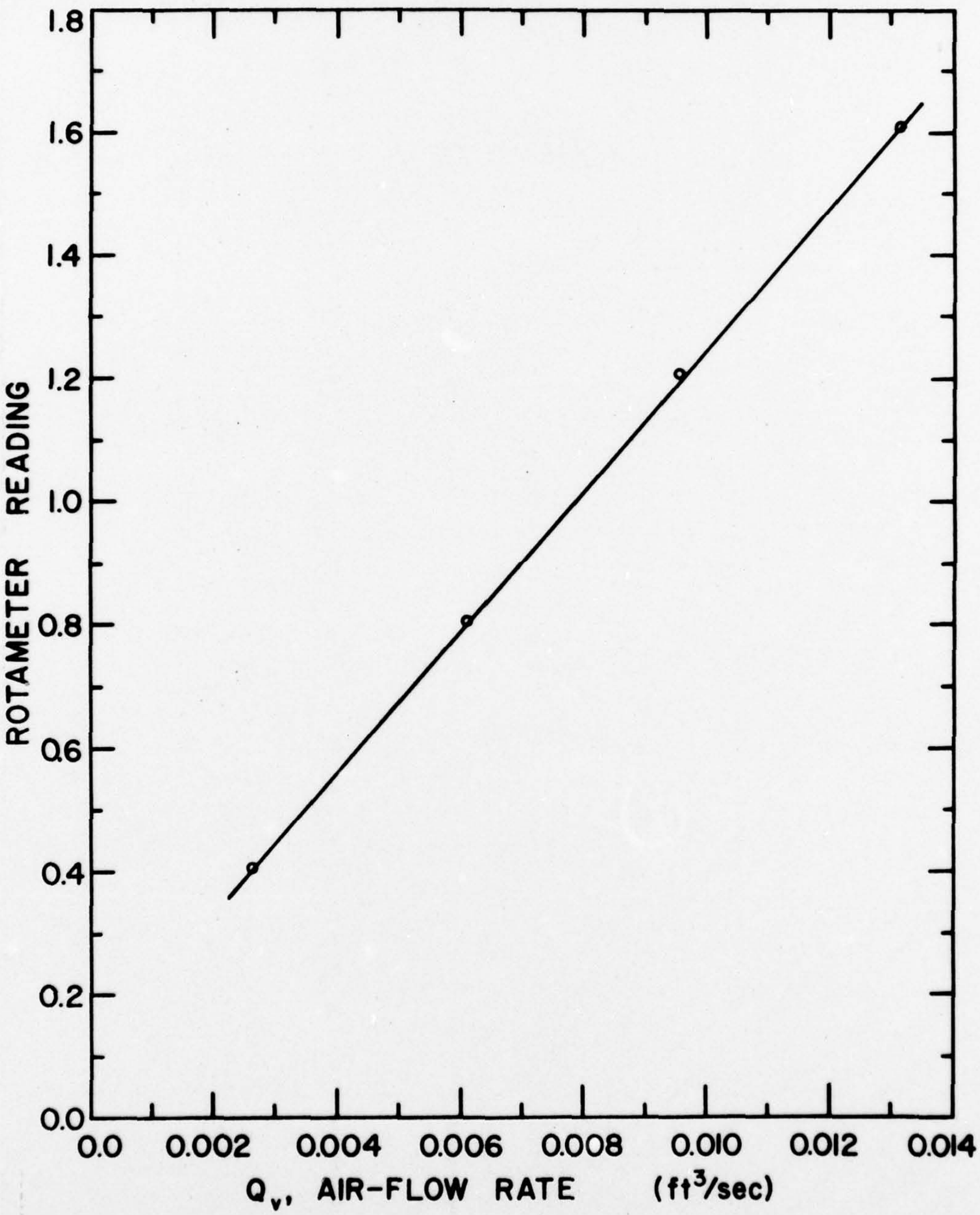

FIGURE 2-7. CALIBRATION CURVE FOR THE FISCHER & PORTER 1/4 - 20 - G - 5/81 ROTAMETER WITH BLACK-GLASS-BEAD FLOAT

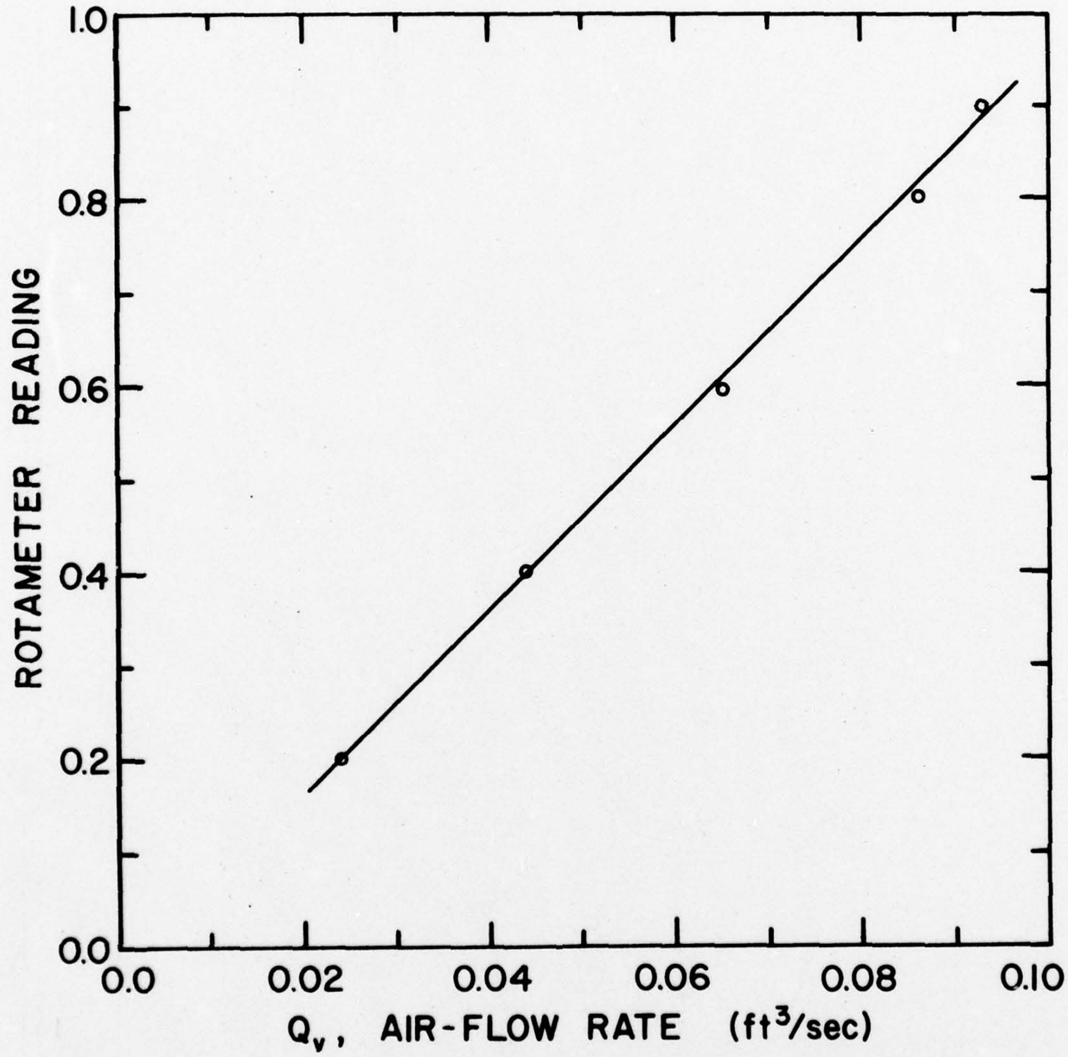

FIGURE 2-8. CALIBRATION CURVE FOR THE FISCHER & PORTER 1/2 - 27 - G - 10/80 ROTAMETER WITH 1/2 - SVT - 45 STAINLESS-STEEL FLOAT

other side of the weir through the 4-inch drain hole. For a constant input flow the height of the water in the drum remained constant, thus providing a constant back pressure. A constant back pressure was necessary to take accurate readings both across the impeller and for the venturi.

CHAPTER 3

EXPERIMENTAL PROCEDURE

SINGLE-PHASE CHARACTERISTIC TESTS

With the plastic impeller in use, 26 single-phase data points were obtained while 28 points were obtained using the bronze impeller. The method used to obtain the data from both of the impellers was the same. A constant speed was set on the variable-speed motor and checked by the use of the Strobotac. The water-flow rate was then adjusted to an appropriate value on the 60-inch manometer, and determined from the venturi calibration curve. For each setting of pump speed and water-flow rate the corresponding static head across the pump was read off the 30-inch manometer. Speeds of 190, 250, 318 and 390 rev/min and flow rates of 0.0 to 46.0 gal/min were tested using the plastic impeller. With the bronze impeller, speeds of 200, 300, 350 and 400 rev/min and flow rates of 0.0 to 50.0 gal/min were tested. Care was taken to allow the back pressure to reach a steady value (constant water height in the exit drum) and to eliminate any air bubbles in the manometer lines before any readings were taken.

The shut-off head was determined for the various speeds by blocking the drum drain hole, shutting off the flow, and allowing the water in the drum and in the inlet piping to

achieve a level configuration. The motor was then turned on, pumping the water to a higher level in the drum and lowering the level in the inlet piping. When a steady-state level was attained, the difference in height between the water level in the drum and that viewed in the Plexiglass inlet pipe was the shut-off head.

Since the correlation proposed by Mikielewicz and Wilson is based upon a head-loss ratio employing total heads, the dynamic head across the pump had to be calculated and added to the measured static heads in order to obtain the actual total single-phase head, ΔH_{osp}. The dynamic head was calculated in the following manner.

$$H_{dyn\ sp} \equiv \frac{C^2}{2g} = \left(\frac{Q}{A}\right)^2 \times \frac{1}{2g}$$

where $H_{dyn\ sp} \equiv$ single-phase dynamic head.

Therefore,

$$H_{dyn\ sp1} = \left(\frac{Q}{A_1}\right)^2 \times \frac{1}{2g} \qquad H_{dyn\ sp2} = \left(\frac{Q}{A_2}\right)^2 \times \frac{1}{2g}$$

and

$$\Delta H_{dyn\ sp} \equiv H_{dyn\ sp2} - H_{dyn\ sp1} = \left(\frac{Q^2}{2g}\right)\left[\frac{1}{A_2^{\,2}} - \frac{1}{A_1^{\,2}}\right]$$

where for the plastic impeller $A_1 = 0.0123\ ft^2$

$A_2 = 0.0324\ ft^2$

and for the bronze impeller $A_1 = 0.0341\ ft^2$

$$A_2 = 0.0324\ ft^2$$

Having obtained a value of ΔH_{osp} for each of the data points recorded, a plot of head coefficient, ψ', versus flow coefficient, ϕ, was then made.

$$\text{Head coefficient} \equiv \psi' \equiv \frac{g\Delta H_o}{u^2}$$

$$\text{Flow coefficient} \equiv \phi \equiv \frac{c_m}{u}$$

The first-quadrant single-phase pump characteristic curves obtained by actual data plotting are shown in figures 3-1 and 3-2 for the plastic and bronze impellers respectively. The single-phase data used to construct these curves are listed in tables 3-1 and 3-2 respectively.

The data from the bronze impeller were run on a curve-fitting computer program (reference 3-1, Appendix E) and the resulting curve-fitted plot is shown in figure 3-3. The equation for the curve in figure 3-3 is as follows.

$$\psi'_{sp} = 0.413 + 0.580\ \phi_2 - 5.772\ \phi_2^{\ 2} - 614.27\ \phi_2^{\ 3} + 17931.1\ \phi_2^{\ 4} - 48526.0\ \phi_2^{\ 5} + 106810.0\ \phi_2^{\ 6} \quad (3\text{-}1)$$

TWO-PHASE CHARACTERISTIC TESTS

Before two-phase data could be obtained from the test facility a method of calculating void fraction had to be

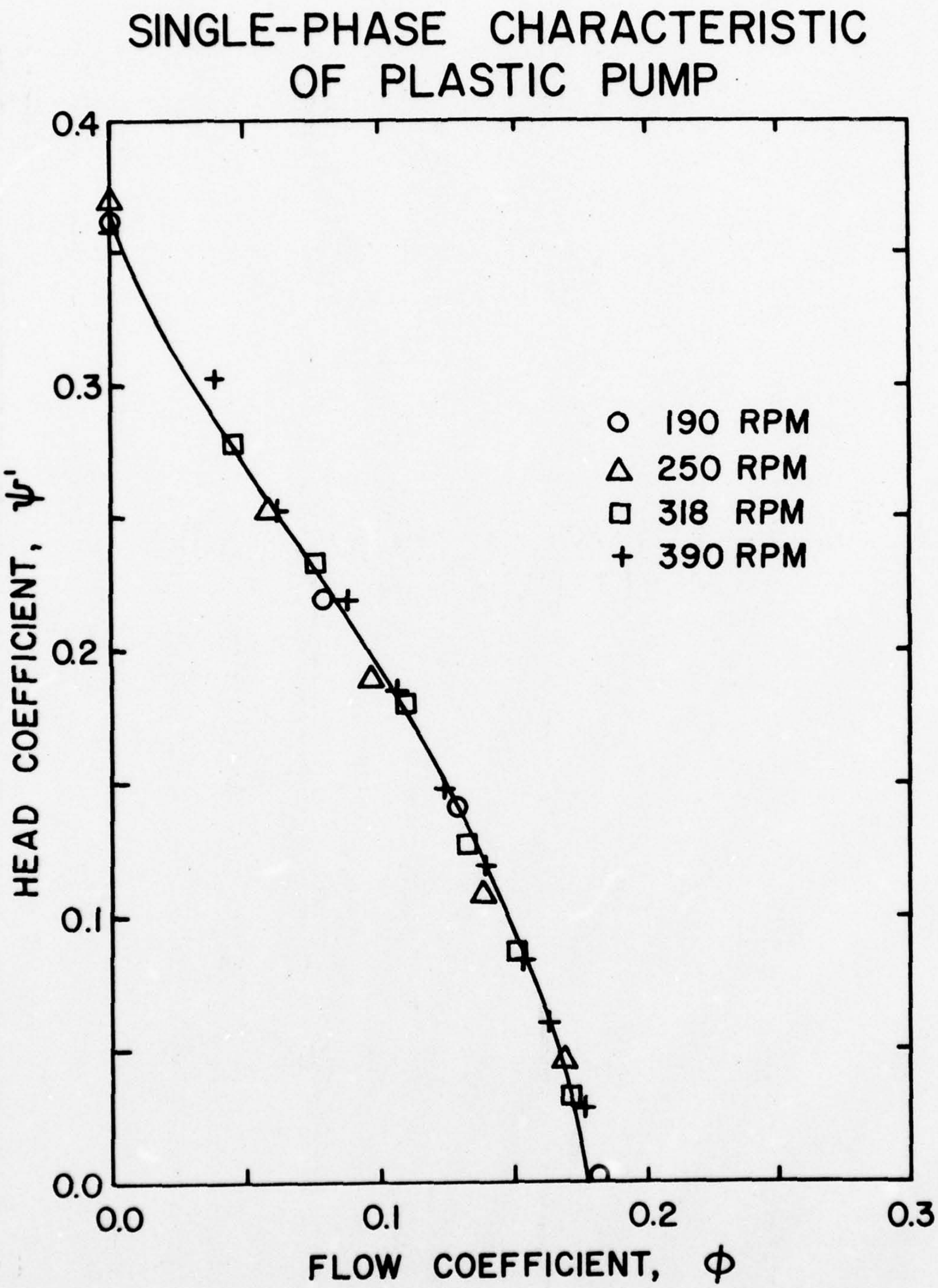

FIGURE 3-1. SINGLE-PHASE CHARACTERISTIC OF THE PLASTIC IMPELLER

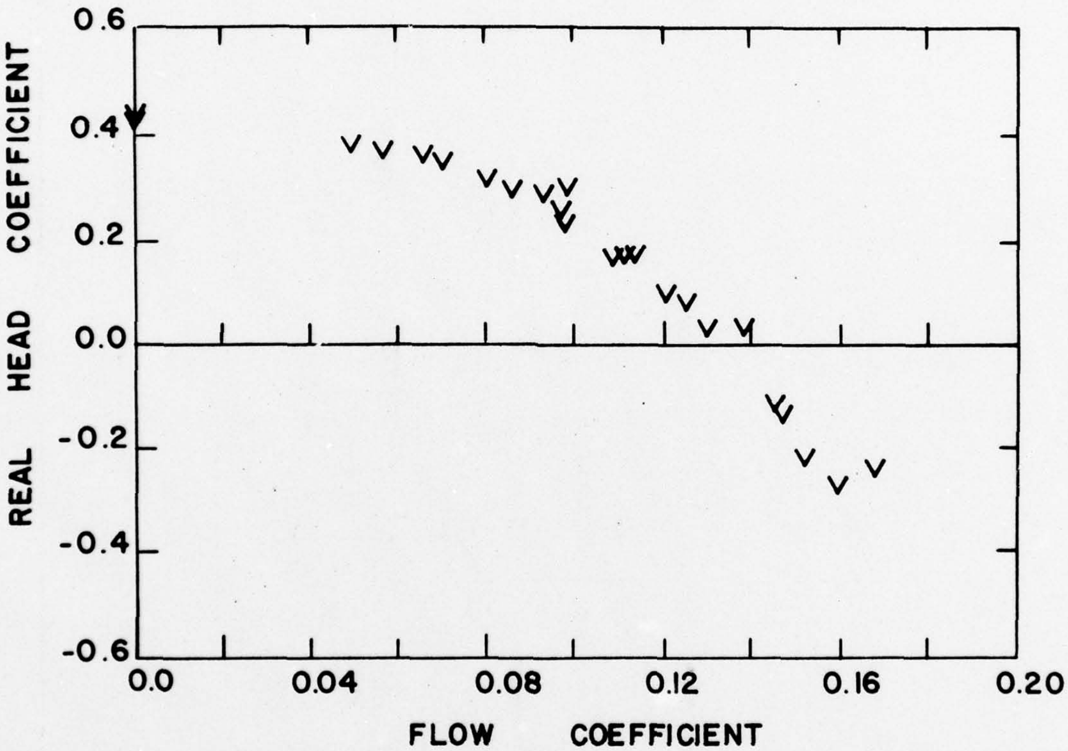

FIGURE 3-2. SINGLE-PHASE CHARACTERISTIC OF THE BRONZE IMPELLER

TABLE 3-1

SINGLE-PHASE PLASTIC-IMPELLER DATA

MOTOR SPEED (rpm)	TEST NO.	WATER-FLOW RATE (ft^3/sec)	TOTAL HEAD (in. H_2O)	FLOW COEFF. ϕ	HEAD COEFF. ψ'
190	01	0.0	6.25	0.0	0.3640
	02	0.0223	3.78	0.0787	0.220
	03	0.0361	2.43	0.1276	0.1412
	04	0.0512	0.03	0.1811	0.0017
250	05	0.0	11.0	0.0	0.370
	06	0.023	7.58	0.0598	0.2549
	07	0.0361	5.63	0.0969	0.1892
	08	0.0512	3.23	0.1376	0.1086
	09	0.0624	1.39	0.1676	0.0468
318	10	0.0	17.75	0.0	0.3690
	11	0.0223	13.38	0.0470	0.2781
	12	0.0361	11.23	0.0762	0.2334
	13	0.0512	8.73	0.1082	0.1815
	14	0.0624	6.09	0.1317	0.1267
	15	0.0719	4.17	0.1515	0.0868
	16	0.0806	1.55	0.1703	0.0323
390	17	0.0	26.0	0.0	0.3590
	18	0.0223	21.73	0.0384	0.0300
	19	0.0361	18.33	0.0621	0.2533
	20	0.0512	15.93	0.0882	0.2202

TABLE 3-1 (continued)

MOTOR SPEED (rpm)	TEST NO.	WATER-FLOW RATE (ft^3/sec)	TOTAL HEAD (in. H_2O)	FLOW COEFF. ϕ	HEAD COEFF. ψ'
390	21	0.0624	13.39	0.1074	0.1851
	22	0.0719	10.77	0.1239	0.1489
	23	0.0806	8.74	0.1389	0.1208
	24	0.0888	6.20	0.1527	0.0857
	25	0.0950	4.48	0.1627	0.0620
	26	0.1024	2.07	0.1761	0.0285

TABLE 3-2

SINGLE-PHASE BRONZE-IMPELLER DATA

MOTOR SPEED (rpm)	TEST NO.	WATER-FLOW RATE (ft^3/sec)	TOTAL HEAD (in. H_2O)	FLOW COEFF. ϕ	HEAD COEFF. ψ'
200	01	0.0	6.5	0.0	0.4283
	02	0.0361	4.32	0.0974	0.2847
	03	0.0512	0.25	0.1381	0.0165
	04	0.0624	-3.73	0.1684	-0.2458
	05	0.0719	-9.11	0.1940	-0.6003
300	06	0.0	14.13	0.0	0.4138
	07	0.0361	12.0	0.0649	0.3514
	08	0.0512	9.4	0.0921	0.2753
	09	0.0624	5.3	0.1122	0.1552
	10	0.0719	0.39	0.1293	0.0114
	11	0.0806	-4.39	0.1450	-0.1286
	12	0.0886	-9.57	0.1594	-0.2803
350	13	0.0361	16.52	0.0557	0.3555
	14	0.0512	14.05	0.0789	0.3023
	15	0.0624	11.37	0.0962	0.2446
	16	0.0719	7.19	0.1109	0.1547
	17	0.0806	3.11	0.1243	0.0669
	18	0.0886	-1.67	0.1366	-0.0359
	19	0.0953	-6.55	0.1469	-0.1409

TABLE 3-2 (continued)

MOTOR SPEED (rpm)	TEST NO.	WATER-FLOW RATE (ft^3/sec)	TOTAL HEAD (in. H_2O)	FLOW COEFF. ϕ	HEAD COEFF. ψ'
400	20	0.0	24.63	0.0	0.4057
	21	0.0361	22.62	0.0487	0.3726
	22	0.0512	20.35	0.0691	0.3352
	23	0.0624	17.17	0.0842	0.2829
	24	0.0719	13.29	0.0970	0.2189
	25	0.0806	9.51	0.1087	0.1567
	26	0.0886	5.03	0.1195	0.0829
	27	0.0953	0.45	0.1286	0.0074
	28	0.1022	-4.42	0.1379	-0.0728

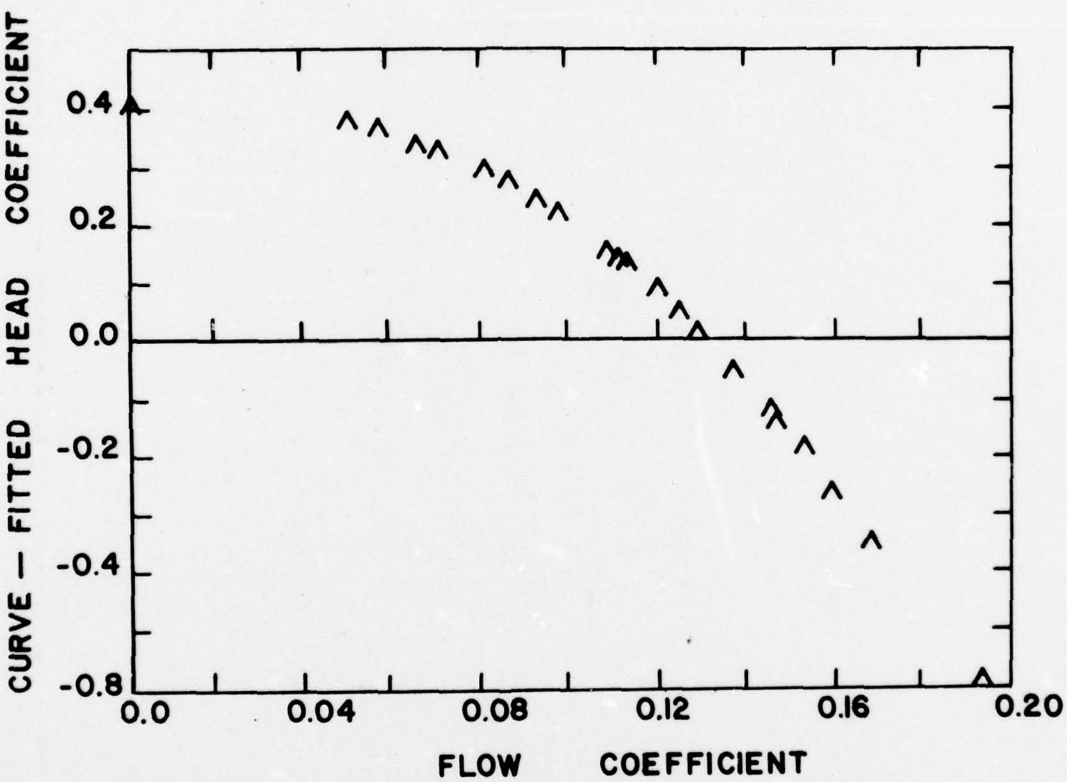

FIGURE 3-3. CURVE-FITTED SINGLE-PHASE CHARACTERISTIC OF THE BRONZE IMPELLER

established. Since the air and water may travel at different velocities throughout the system, the void fraction cannot be inferred from a ratio of the respective inlet volume flows. The method chosen for calculating the void fraction during these tests was based on the drift-flux model of two-phase flow developed by Zuber and Wallis (reference 3-2). The drift-flux model satisfactorily accounts for the influence of mass velocity on the void fraction as seen in the separated-flow model, and is useful in the bubbly-, slug-, and churn-flow regimes. These flow regimes include void fractions from 0.0 to approximately 0.80. The specific equation developed from the drift-flux model used to calculate void fractions throughout the experiment is given below (reference 3-3).

$$\alpha = \frac{Q_V}{1.2(Q_V+Q_L)-0.35(gd)^{1/2}A_1} \tag{3-2}$$

where $d \equiv$ inlet-pipe diameter

$= 0.125$ ft. for the plastic impeller

$= 0.2083$ ft. for the bronze impeller

and $A_1 \equiv$ inlet-pipe area.

The details of the void-fraction calculation using the drift-flux model are contained in Appendix D.

Using equation 3-1, for a water-flow rate, Q_L, an appropriate air-flow rate, Q_V, was determined for a specified

void fraction. Thus, by setting appropriate values of Q_L and Q_v, a void-fraction range of 0.0 to 0.62 was obtained during the experiment.

The acquisition of the two-phase data proceeded in much the same manner as that of the single-phase data. A speed was set by adjusting the traction-drive ratio of the impeller motor, and checked by the Strobotac. Using the venturi and rotameter calibration curves, appropriate water- and air-flow rates were set to yield desired void fractions. For each value of void fraction at different Q_L and Q_v the static head across the impeller was read off the 30-inch manometer and recorded. Again, care was taken to allow the back pressure to attain a steady value, and to remove any air bubbles in the manometer lines before readings were taken. Using the plastic impeller the above procedure was repeated for 190, 250, 318 and 390 rev/min, and for water-flow rates of 10.0 to 46.0 gal/min, covering a void-fraction range of 0.0 to 0.62. Using the bronze impeller this procedure was repeated for 200, 300, 350 and 400 rev/min, and for water-flow rates of 10.0 to 50.0 gal/min, covering a void-fraction range of 0.0 to 0.40.

Having obtained the static head across the pump from the 30-inch-manometer reading, the dynamic head had to be calculated so that the total two-phase head could be used in the correlation. The calculation of the total two-phase head

was based upon an effective two-phase density (reference 3-4), ρ_{tp}, taking slip between the vapor and liquid phases into consideration. The details of the two-phase dynamic-head calculations are given in Appendix C. The total two-phase head across the pump was then determined by the following equation.

$$\Delta H_{otp} = \Delta H_{tp} + \frac{\rho_{L2}\left(\frac{Q_{L2}}{(1-\alpha)A_2}\right)^2 - \rho_{L1}\left(\frac{Q_{L1}}{(1-\alpha)A_1}\right)^2}{2g\rho_{tp}}$$

where

$$\rho_{tp} = \frac{\rho_v \alpha s + (1-\alpha)\rho_L}{(1-\alpha) + \alpha s} \; ; \qquad s \equiv \frac{J_v(1-\alpha)}{J_L \alpha}$$

In this manner the total head across the pump was calculated for 63 two-phase data points obtained from the plastic impeller, and 50 two-phase data points obtained from the bronze impeller.

Having obtained a value of ΔH_{otp} for each of the two-phase data points recorded, the head coefficient, ψ'_{tp}, and the flow coefficient, ϕ_{tp}, were calculated and recorded for each data point. Lists of the two-phase data taken from both the plastic and bronze impeller are given in tables 3-3 and 3-4 respectively.

TABLE 3-3

TWO-PHASE PLASTIC-IMPELLER DATA

MOTOR SPEED (rpm)	TEST NO.	VOID FRACTION α	WATER-FLOW RATE (ft^3/sec)	AIR-FLOW RATE (ft^3/sec)	TOTAL HEAD (in. H_2O)	FLOW COEFF. ϕ	HEAD COEFF. ψ'
190	01	0.10	0.0223	0.0021	-1.81	0.0861	-0.1054
	02	0.15	0.0223	0.0033	-2.24	0.0906	-0.1305
	03	0.20	0.0223	0.0048	-2.60	0.0957	-0.1514
	04	0.25	0.0223	0.0065	-4.01	0.1017	-0.2335
	05	0.30	0.0223	0.0085	-4.49	0.1089	-0.2615
	06	0.40	0.0223	0.0140	-5.98	0.1282	-0.3483
	07	0.10	0.0361	0.0039	-3.09	0.1415	-0.1700
	08	0.15	0.0361	0.0064	-4.95	0.1500	-0.2883
	09	0.20	0.0361	0.0091	-6.10	0.1599	-0.3553
	10	0.25	0.0361	0.0124	-6.90	0.1714	-0.4019
250	18	0.10	0.0223	0.0021	-1.81	0.0654	-0.0609
	19	0.15	0.0223	0.0033	-2.24	0.0687	-0.0754
	20	0.20	0.0223	0.0048	-3.30	0.0727	-0.1110
	21	0.25	0.0223	0.0065	-3.81	0.0773	-0.1282
	22	0.30	0.0223	0.0085	-4.39	0.0829	-0.1477
	23	0.40	0.0223	0.0140	-5.98	0.0974	-0.2012
	24	0.10	0.0361	0.0039	-3.99	0.1076	-0.1342
	25	0.15	0.0361	0.0064	-4.85	0.1141	-0.1632
	26	0.20	0.0361	0.0091	-5.80	0.1215	-0.1951
	27	0.25	0.0361	0.0124	-7.00	0.1303	-0.2355
	28	0.10	0.0512	0.0060	-5.03	0.1537	-0.1692
	29	0.15	0.0512	0.0097	-6.47	0.1635	-0.2176
	30	0.20	0.0512	0.0139	-7.82	0.1749	-0.2631
318	35	0.10	0.0223	0.0021	2.19	0.0515	0.0455
	36	0.15	0.0223	0.0021	0.86	0.0541	0.0179

TABLE 3-3 (continued)

MOTOR SPEED (rpm)	TEST NO.	VOID FRACTION α	WATER-FLOW RATE (ft^3/sec)	AIR-FLOW RATE (ft^3/sec)	TOTAL HEAD (in. H_2O)	FLOW COEFF. ϕ	HEAD COEFF. ψ'
318	37	0.20	0.0223	0.0021	-2.80	0.0572	-0.0582
	38	0.25	0.0223	0.0065	-3.91	0.0608	-0.0813
	39	0.30	0.0223	0.0085	-4.59	0.0651	-0.0954
	40	0.40	0.0223	0.0140	-6.18	0.0766	-0.1285
	41	0.10	0.0361	0.0039	0.61	0.0846	0.0127
	42	0.15	0.0361	0.0064	-4.75	0.0897	-0.0988
	43	0.20	0.0361	0.0091	-5.70	0.0955	-0.1185
	44	0.25	0.0361	0.0124	-7.00	0.1025	-0.1455
	45	0.10	0.0512	0.0060	-1.63	0.1208	-0.0339
	46	0.15	0.0512	0.0097	-7.07	0.1286	-0.1470
	47	0.20	0.0512	0.0139	-8.52	0.1375	-0.1771
	48	0.10	0.0719	0.0088	-6.69	0.1705	-0.1391
390	52	0.10	0.0223	0.0021	2.39	0.0420	0.0330
	53	0.15	0.0223	0.0033	-2.14	0.0441	-0.0296
	54	0.20	0.0223	0.0045	-2.80	0.0466	-0.0387
	55	0.25	0.0223	0.0065	-3.41	0.0496	-0.0434
	56	0.30	0.0223	0.0085	-4.69	0.0531	-0.0648
	57	0.40	0.0223	0.014	-5.88	0.0625	-0.0813
	58	0.10	0.0361	0.0039	2.71	0.0690	0.0375
	59	0.15	0.0361	0.0064	- .05	0.0731	-0.0007
	60	0.20	0.0361	0.0091	-6.20	0.0779	-0.0857
	61	0.25	0.0361	0.0124	-6.90	0.0835	-0.0954
	62	0.10	0.0512	0.0060	.37	0.0985	0.0051
	63	0.15	0.0512	0.0097	-6.87	0.1048	-0.0950
	64	0.20	0.0512	0.0139	-8.12	0.1121	-0.1122
	65	0.10	0.0719	0.0088	-3.79	0.1391	-0.0524
	66	0.15	0.0719	0.0142	-2.08	0.1483	-0.1670

TABLE 3-3 (continued)

MOTOR SPEED (rpm)	TEST NO.	VOID FRACTION α	WATER-FLOW RATE (ft^3/sec)	AIR-FLOW RATE (ft^3/sec)	TOTAL HEAD (in. H_2O)	FLOW COEFF. ϕ	HEAD COEFF. ψ'
390	67	0.10	0.0886	0.0111	-4.35	0.1717	-0.0602
190	69	0.51	0.0223	0.0233	-8.28	0.1612	-0.4822
250	70	0.51	0.0223	0.0233	-8.28	0.1225	-0.2785
	71	0.62	0.0223	0.0439	-14.67	0.1779	-0.4935
	72	0.37	0.0361	0.0233	-9.52	0.1596	-0.3203
318	73	0.51	0.0223	0.0233	-7.78	0.0963	-0.1618
	74	0.62	0.0223	0.0439	-14.27	0.1398	-0.2967
	75	0.37	0.0361	0.0233	-9.52	0.1255	-0.1979
	76	0.50	0.0361	0.0439	-16.40	0.1689	-0.3410
	77	0.29	0.0512	0.0233	-11.41	0.1574	-0.2372
	79	0.25	0.0624	0.0233	-13.47	0.1810	-0.2801

TABLE 3-4

TWO-PHASE BRONZE-IMPELLER DATA

MOTOR SPEED (rpm)	TEST NO.	VOID FRACTION α	WATER-FLOW RATE (ft^3/sec)	AIR-FLOW RATE (ft^3/sec)	TOTAL HEAD (in. H_2O)	FLOW COEFF. ϕ	HEAD COEFF. ψ'
200	01	0.15	0.0361	0.0023	-2.77	0.1036	-0.1825
	02	0.20	0.0361	0.0033	-3.16	0.1063	-0.2082
	03	0.25	0.0361	0.0044	-3.86	0.1092	-0.2544
	04	0.10	0.0512	0.0035	-4.54	0.1475	-0.2992
	05	0.15	0.0512	0.0056	-10.43	0.1532	-0.6873
	06	0.20	0.0512	0.0080	-12.42	0.1597	-0.8184
300	07	0.15	0.0361	0.0023	-0.97	0.0691	-0.0284
	08	0.20	0.0361	0.0033	-1.96	0.0709	-0.0574
	09	0.25	0.0361	0.0044	-2.66	0.0728	-0.0779
	10	0.10	0.0512	0.0035	-3.84	0.0984	-0.1125
	11	0.15	0.0512	0.0056	-10.73	0.1021	-0.3142
	12	0.20	0.0512	0.0080	-11.32	0.1065	-0.3315
	13	0.10	0.0719	0.0063	-12.08	0.1406	-0.3538
	14	0.15	0.0719	0.0101	-23.86	0.1475	-0.6988
	15	0.10	0.0886	0.0086	-16.52	0.1748	-0.4838
350	16	0.15	0.0361	0.0023	-0.47	0.0592	-0.0101
	17	0.20	0.0361	0.0033	-0.76	0.0607	-0.0164
	18	0.25	0.0361	0.0044	-0.96	0.0624	-0.0207
	19	0.10	0.0512	0.0035	-3.44	0.0843	-0.0740
	20	0.15	0.0512	0.0056	-9.93	0.0875	-0.2137
	21	0.20	0.0512	0.0080	-10.92	0.0912	-0.2350
	22	0.10	0.0719	0.0063	-8.28	0.1205	-0.1782
	23	0.15	0.0719	0.0101	-23.36	0.1264	-0.5026
	24	0.10	0.0886	0.0086	-10.82	0.1498	-0.2328
	25	0.10	0.1022	0.0104	-21.55	0.1736	-0.4637

TABLE 3-4 (continued)

MOTOR SPEED (rpm)	TEST NO.	VOID FRACTION α	WATER-FLOW RATE (ft^3/sec)	AIR-FLOW RATE (ft^3/sec)	TOTAL HEAD (in. H_2O)	FLOW COEFF. ϕ	HEAD COEFF. ψ'
400	26	0.15	0.0361	0.0023	-0.23	0.0518	0.0038
	27	0.20	0.0361	0.0033	-0.26	0.0531	-0.0043
	28	0.25	0.0361	0.0044	-0.36	0.0546	-0.0059
	29	0.10	0.0512	0.0035	-3.24	0.0738	-0.0534
	30	0.15	0.0512	0.0056	-7.23	0.0766	-0.1191
	31	0.20	0.0512	0.0080	-7.72	0.0798	-0.1272
	32	0.10	0.0719	0.0063	-5.08	0.1055	-0.0837
	33	0.15	0.0719	0.0101	-21.66	0.1106	-0.3568
	34	0.10	0.0886	0.0086	-5.82	0.1311	-0.0959
	35	0.10	0.1022	0.0104	-15.55	0.1519	-0.2562
200	36	0.30	0.0361	0.0058	-4.15	0.1130	-0.2735
	37	0.40	0.0361	0.0095	-4.72	0.1230	-0.3110
	38	0.10	0.0624	0.0050	-8.11	0.1818	-0.5344
300	40	0.30	0.0361	0.0058	-2.85	0.0753	-0.0835
	41	0.40	0.0361	0.0095	-4.02	0.0820	-0.1177
	42	0.10	0.0624	0.0050	-5.81	0.1212	-0.1702
	43	0.20	0.0624	0.0116	-19.98	0.1331	-0.5851
350	44	0.30	0.0361	0.0058	-1.25	0.0646	-0.0269
	45	0.40	0.0361	0.0095	-1.92	0.0703	-0.0413
	46	0.10	0.0624	0.0050	-4.71	0.1039	-0.1013
	47	0.20	0.0624	0.0116	-17.48	0.1141	-0.3761
400	48	0.30	0.0361	0.0058	-0.35	0.0565	-0.0058
	49	0.40	0.0361	0.0095	-1.02	0.0615	-0.0168
	50	0.10	0.0624	0.0050	-3.51	0.0909	-0.0578
	51	0.20	0.0624	0.0116	-14.58	0.0998	-0.2402

CHAPTER 4

DERIVATION OF THEORETICAL CHARACTERISTICS

SINGLE PHASE

The first step in determining the theoretical single-phase pump characteristic was to apply Euler's turbomachinery equation to express the change in enthalpy of, or work done on, the fluid flowing through the pump, to the change in moment of momentum of the rotor inlet and outlet flows. In applying Euler's equation, one-dimensional steady flow was assumed. Euler's equation for adiabatic flow can be expressed mathematically as follows.

$$\dot{W}/\dot{m} = g_c(h_{o2} - h_{o1}) \equiv g_c\Delta h_o = u_2C_{\theta 2} - u_1C_{\theta 1} \qquad (4\text{-}1)$$

Since a flow-straightener was used in the inlet piping and inlet swirl vanes were not used throughout the experiment, $C_{\theta 1} = 0$ and equation 4-1 can be simplified to

$$g_c\Delta h_o = u_2C_{\theta 2}$$

For single-phase flow, the simple (one-dimensional) velocity triangles at the rotor tips of the plastic and bronze impellers are shown in figures 4-1 and 4-2 respectively. The angle β_2 is the relative flow angle at the rotor-outlet diameter, and is equal to the rotor blade angle, β_2', less the slip angle, δ. The slip angle for each of the impellers was calculated using the Busemann slip-factor

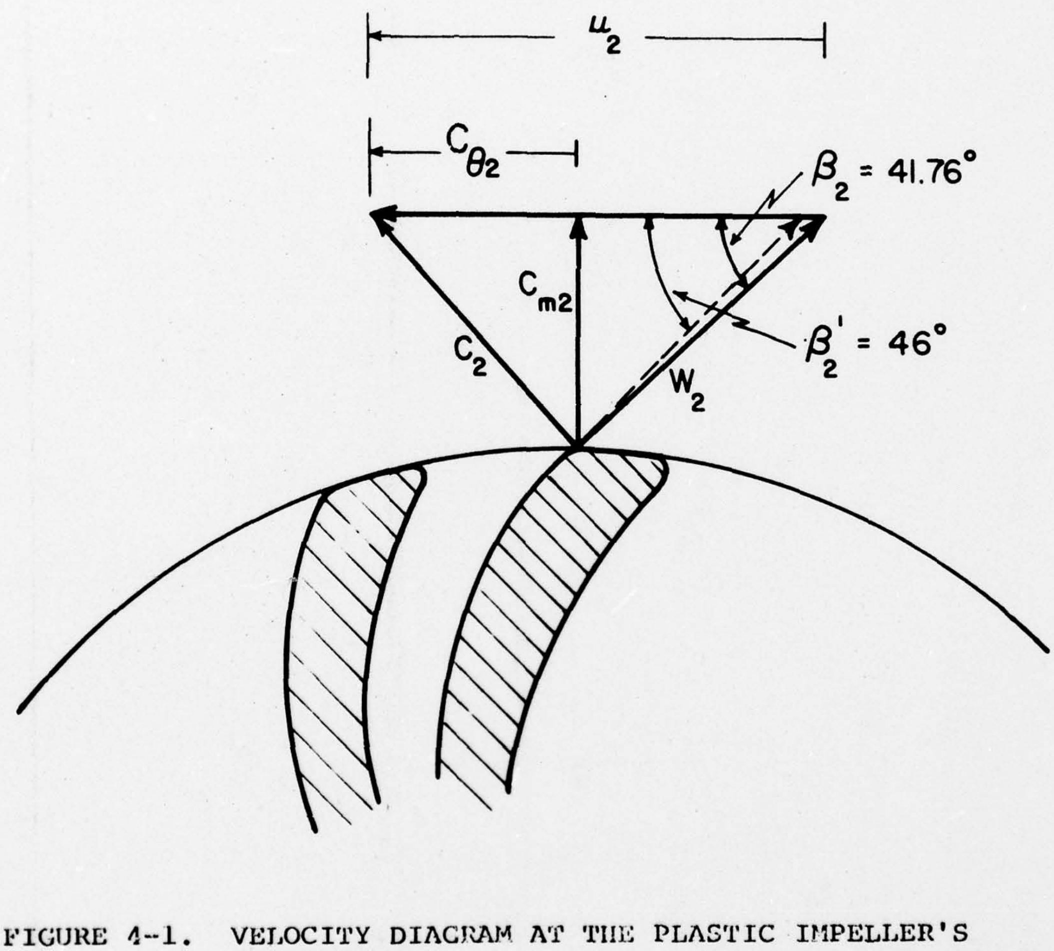

FIGURE 4-1. VELOCITY DIAGRAM AT THE PLASTIC IMPELLER'S BLADE TIP

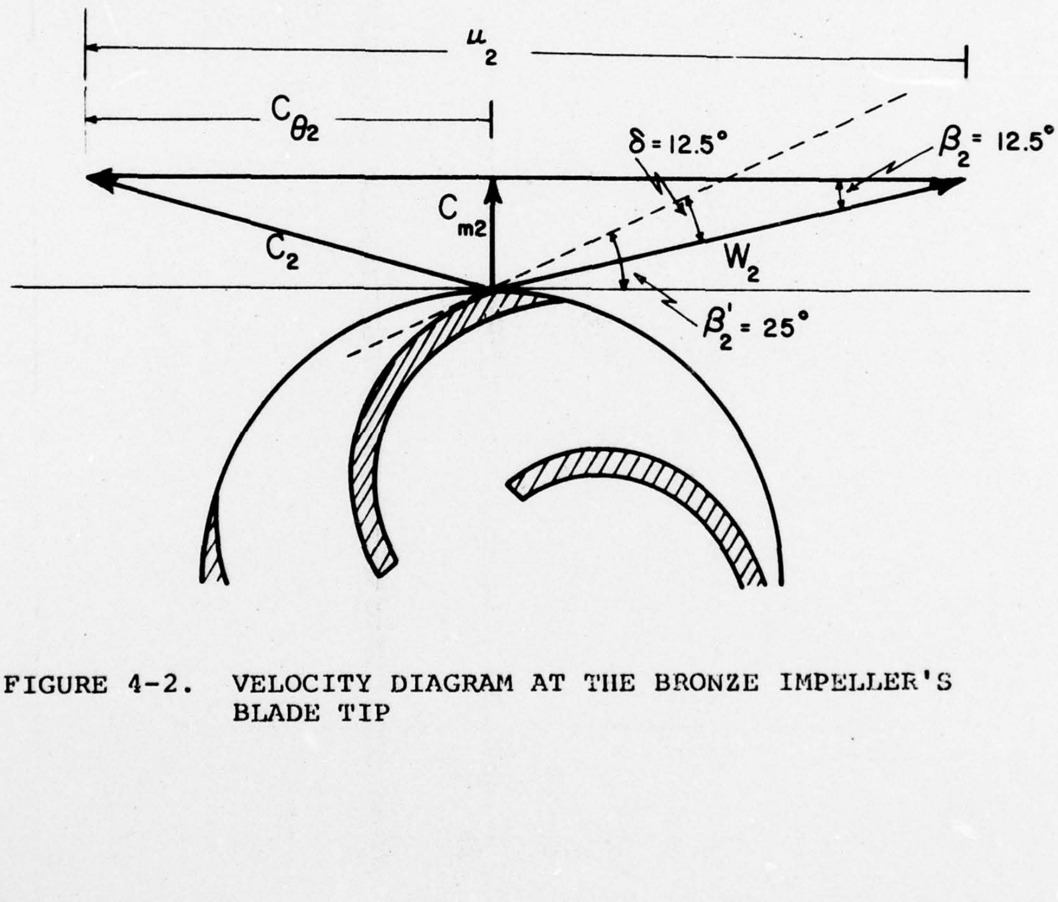

FIGURE 4-2. VELOCITY DIAGRAM AT THE BRONZE IMPELLER'S BLADE TIP

correlation. The details of these calculations can be found in Appendix A. The results of these calculations were $\beta_2 = 41.76°$ for the plastic impeller, and $\beta_2 = 12.5°$ for the bronze impeller.

From the geometry of the velocity triangles

$$C_{\theta 2} = u_2 - \frac{C_{m2}}{\tan \beta_2}$$

Therefore,

$$g_c \Delta h_o = u_2^2 - \frac{u_2 C_{m2}}{\tan \beta_2} \tag{4-2}$$

Dividing through equation 4-2 by u_2^2 yields

$$\frac{g_c \Delta h_o}{u_2^2} = 1.0 - \frac{C_{m2}}{u_2} \times \frac{1}{\tan \beta_2}$$

Now, for the specific case of loss-less incompressible flow, the theoretical total-enthalpy change is proportional to the theoretical total-head change. Thus, ths expression for the theoretical single-phase pump characteristic is

$$\frac{g \Delta H_o}{u_2^2} = \frac{g_c \Delta h_o}{u_2^2} = 1.0 - \frac{C_{m2}}{u_2} \times \frac{1}{\tan \beta_2} \tag{4-3}$$

Now, employing the definitions of flow coefficient,

$$\phi \equiv \frac{C_m}{u}$$

and head coefficient,

$$\psi' \equiv \frac{g \Delta H_o}{u_2^2}$$

equation 4-3 becomes

$$\psi'_{spth} = 1.0 - \frac{\phi_2}{\tan \beta_2} \tag{4-4}$$

For the plastic impeller, using Busemann's slip-factor correlation and the geometry of the impeller, the theoretical single-phase characteristic curve, in the form of equation 4-4, was determined to be

$$\psi'_{spth} = 1.0 - 1.120014\ \phi_2 \tag{4-5}$$

Following the same procedure, the theoretical single-phase characteristic curve equation for the bronze impeller was calculated to be

$$\psi'_{spth} = 1.0 - 4.511\ \phi_2 \tag{4-6}$$

TWO PHASE

The Euler equation is applicable to both single- and two-phase flow. However, in two-phase flow there are two separate mass flows with presumably different tangential and radial velocities at both rotor inlet and outlet. Euler's equation for two-phase flow with zero inlet swirl then becomes

$$\psi'_{tpth} = (1-x_2)\ \frac{C_{\theta L2}}{u_2} + x_2\ \frac{C_{\theta v2}}{u_2} \tag{4-7}$$

From the geometry of the velocity triangles at the rotor outlet, equation 4-7 can be transformed to

$$\psi'_{tpth} = (1-x_2)[1.0 - \frac{C_{mL2}}{(u_2 \tan \beta_2)}] + x_2[1.0 - \frac{C_{mv2}}{(u_2 \tan \beta_2)}]$$

where the vapor and liquid phases are assumed to leave the rotor at the same relative angle. There may in fact be some difference in their direction, but the effect will be small (reference 4-1).

Substituting for

$$C_{mL2} = \dot{m}_{L2}/(\rho_{L2}A_{L2}) = \dot{m}_T(1-x_2)/[\rho_{L2}(1-\alpha_2)A_{T2}]$$

$$C_{mv2} = \dot{m}_{v2}/(\rho_{v2}A_{v2}) = \dot{m}_T x_2/[\rho_{v2}\alpha_2 A_{T2}]$$

and defining a two-phase flow coefficient

$$\phi_{tp} \equiv \frac{Q_{tp}}{Au} = \dot{m}_T/(\rho_{tp}Au)$$

where the mean two-phase density is defined as

$$\rho_{tp} \equiv (1-\alpha)\rho_L + \alpha\rho_v$$

then

$$\psi'_{tpth} = 1.0 - \frac{\phi_{tp2}}{\tan \beta_2} [1.0 + \frac{\alpha_2}{(1-\alpha_2)} \frac{\rho_{v2}}{\rho_{L2}}]$$

$$[(1-x_2)^2 + \frac{(1-\alpha_2)}{\alpha_2} \frac{\rho_{L2}}{\rho_{v2}} x_2{}^2]$$

Defining a two-phase flow function,

$$a \equiv (\alpha/(1-\alpha)(\rho_v/\rho_L)$$

a slip velocity ratio,

$$s \equiv C_V/C_L$$

and quality,

$$x = as/(1 + as)$$

it can be shown (reference 4-2) that the theoretical two-phase characteristic equation for a centrifugal pump with zero inlet swirl becomes

$$\psi'_{tpth} = 1.0 - f_{tp2} \frac{\phi_{tp2}}{\tan \beta_2} \qquad (4\text{-}8)$$

where

$$f_{tp} \equiv \frac{(1 + a)(1 + as^2)}{(1 + as)^2}$$

Equation 4-8 is applicable to both single- and two-phase flow. In single-phase flow $\alpha = 0 = a$, and $f_{th} = 1.0$, transforming equation 4-8 back into equation 4-6 previously developed for single-phase flow.

Substituting the appropriate values for all of the two-phase data points taken, using each of the impellers, into a computer program produced by Tak-Chee Stephen Chan (Appendix E) yielded the theoretical two-phase head coefficients for each of the selected data points.

Thus, having calculated the theoretical single- and two-phase characteristic curve equations for both the plastic and bronze impellers, the next step was to determine the head-loss ratio.

CHAPTER 5

CALCULATION OF THE HEAD-LOSS RATIO

The head-loss ratio, H*, the ratio of the flow losses in two-phase flow to those in single-phase flow, was calculated so that it could be plotted versus void fraction and the results compared to the correlation proposed by Mikielewicz and Wilson. Mathematically, the head-loss ratio can be defined as

$$H^* \equiv \frac{\psi'_{tpth} - \psi'_{tp}}{\psi'_{spth} - \psi'_{sp}} \qquad (5\text{-}1)$$

H* for every two-phase data point was then determined in the following manner. Values of ψ'_{tp} were determined from the definition of the head coefficient, the two-phase total-head data, and the impeller geometry. For the plastic impeller, values of ψ'_{sp} were obtained from figure 3-1 for appropriate values of ϕ. For the bronze impeller, values of ψ'_{sp} were calculated by substituting appropriate values of ϕ into equation 3-1. Finally, values of ψ'_{tpth} and ψ'_{spth} were calculated using equations 4-8 and 4-4 respectively, for appropriate values of flow coefficient and β_2.

The values of head-loss ratio, void fraction, and the associated head coefficients used in determining H*, for the data points taken using the plastic impeller, are given in table 5-1. Table 5-2 contains similar results from the bronze-

impeller tests. The values contained in table 5-2 were arrived at through the use of a computer program developed by Tak-Chee Stephen Chan (Appendix E).

TABLE 5-1

CALCULATION OF HEAD-LOSS RATIO FOR THE PLASTIC IMPELLER DATA

TEST NO.	α	ϕ	ψ'_{spth}	ψ'_{sp}	ψ'_{tpth}	ψ'_{tp}	H*
01	0.10	0.0861	0.9036	0.2150	0.9036	-0.1054	1.4653
02	0.15	0.0906	0.8985	0.2070	0.8986	-0.1305	1.4881
03	0.20	0.0957	0.8928	0.1988	0.8928	-0.1514	1.5046
04	0.25	0.1017	0.8861	0.1880	0.8860	-0.2335	1.6037
05	0.30	0.1089	0.8780	0.1750	0.8780	-0.2615	1.6208
06	0.40	0.1282	0.8564	0.1400	0.8564	-0.3483	1.6815
07	0.10	0.1415	0.8415	0.1135	0.8415	-0.1700	1.4031
08	0.15	0.1500	0.8320	0.0945	0.8319	-0.2883	1.5189
09	0.20	0.1599	0.8209	0.0724	0.8209	-0.3553	1.5714
10	0.25	0.1714	0.8080	0.0375	0.8080	-0.4019	1.5702
18	0.10	0.0654	0.9268	0.2465	0.9267	-0.0609	1.4518
19	0.15	0.0687	0.9231	0.2413	0.9229	-0.0754	1.4643
20	0.20	0.0727	0.9186	0.2355	0.9185	-0.1110	1.5072
21	0.25	0.0773	0.9134	0.2290	0.9134	-0.1282	1.5219
22	0.25	0.0773	0.9134	0.2290	0.9134	-0.1282	1.5219
23	0.30	0.0828	0.9073	0.2195	0.9073	-0.1477	1.5339
24	0.10	0.1076	0.8795	0.1780	0.8795	-0.1342	1.4451
25	0.15	0.1141	0.8722	0.1715	0.8723	-0.1632	1.4777
26	0.20	0.1215	0.8639	0.1533	0.8639	-0.1951	1.4902
27	0.25	0.1303	0.8541	0.1375	0.8540	-0.2355	1.5205

TABLE 5-1 (continued)

TEST NO.	α	ϕ	ψ'_{spth}	ψ'_{sp}	ψ'_{tpth}	ψ'_{tp}	H*
28	0.10	0.1537	0.8279	0.0850	0.8279	-0.1692	1.3422
29	0.15	0.1635	0.8169	0.0625	0.8168	-0.2176	1.3712
30	0.20	0.1749	0.8041	0.0245	0.8041	-0.2631	1.3689
35	0.10	0.0515	0.9423	0.2675	0.9424	0.0455	1.3291
36	0.15	0.0541	0.9394	0.2635	0.9394	0.0179	1.3633
37	0.20	0.0572	0.9359	0.2590	0.9360	-0.0582	1.4686
38	0.25	0.0608	0.9319	0.2535	0.9319	-0.0813	1.4935
39	0.30	0.0651	0.9271	0.2470	0.9271	-0.0954	1.5035
40	0.40	0.0766	0.9142	0.2310	0.9142	-0.1285	1.5262
41	0.10	0.0846	0.9053	0.2170	0.9053	0.0127	1.2969
42	0.15	0.0897	0.8995	0.2085	0.8996	-0.0988	1.4447
43	0.20	0.0955	0.8930	0.1990	0.8930	-0.1185	1.4574
44	0.25	0.1025	0.8852	0.1870	0.8853	-0.1455	1.4763
45	0.10	0.1208	0.8647	0.1565	0.8647	-0.0339	1.2688
46	0.15	0.1286	0.8560	0.1400	0.8560	-0.1470	1.4009
47	0.20	0.1375	0.8460	0.1220	0.8460	-0.1771	1.4131
48	0.10	0.1705	0.8090	0.0425	0.8090	-0.1391	1.2369
52	0.10	0.0420	0.9530	0.2825	0.9530	0.0330	1.3722
53	0.15	0.0441	0.9506	0.2800	0.9506	-0.0296	1.4616
54	0.20	0.0466	0.9478	0.2770	0.9478	-0.0387	1.4706
55	0.25	0.0496	0.9445	0.2710	0.9445	-0.0434	1.4669
56	0.30	0.0531	0.9405	0.2650	0.9406	-0.0648	1.4883

TABLE 5-1 (continued)

TEST NO.	α	ϕ	ψ'_{spth}	ψ'_{sp}	ψ'_{tpth}	ψ'_{tp}	H*
57	0.40	0.0625	0.9300	0.2510	0.9301	-0.0813	1.4895
59	0.15	0.0731	0.9181	0.2350	0.9181	-0.0007	1.3450
60	0.20	0.0779	0.9128	0.2275	0.9128	-0.0857	1.4571
61	0.25	0.0835	0.9065	0.2190	0.9064	-0.0954	1.4573
62	0.10	0.0985	0.8897	0.1940	0.8897	0.0051	1.2715
63	0.15	0.1048	0.8826	0.1830	0.8826	-0.0950	1.3973
64	0.20	0.1121	0.8745	0.1710	0.8744	-0.1122	1.4025
65	0.10	0.1391	0.8442	0.1185	0.8443	-0.0524	1.2356
66	0.15	0.1483	0.8339	0.0975	0.8339	-0.1670	1.3592
67	0.10	0.1717	0.8077	0.0375	0.8077	-0.0602	1.1268
69	0.51	0.1612	0.8195	0.0690	0.8234	-0.4822	1.7400
70	0.51	0.1225	0.8628	0.1515	0.8628	-0.2785	1.6045
71	0.62	0.1779	0.8008	0.0075	0.8007	-0.4935	1.6316
72	0.37	0.1596	0.8213	0.0725	0.8212	-0.3203	1.5246
73	0.51	0.0963	0.8921	0.1975	0.8921	-0.1618	1.5172
74	0.62	0.1398	0.8434	0.1175	0.8434	-0.2967	1.5705
75	0.37	0.1255	0.8594	0.1463	0.8595	-0.1979	1.4827
76	0.50	0.1689	0.8108	0.0470	0.8107	-0.3410	1.5078
77	0.29	0.1574	0.8237	0.0780	0.8237	-0.2372	1.4227

TABLE 5-2

CALCULATION OF HEAD-LOSS RATIO FOR THE BRONZE-IMPELLER DATA

TEST NO.	α	ϕ	ψ'_{spth}	ψ'_{sp}	ψ'_{tpth}	ψ'_{tp}	H*
01	0.15	0.1036	0.5328	0.1950	0.5328	-0.1825	2.1173
02	0.20	0.1063	0.5206	0.1800	0.5206	-0.2082	2.1400
03	0.25	0.1092	0.5072	0.1629	0.5072	-0.2544	2.2118
04	0.10	0.1475	0.3345	-0.1324	0.3345	-0.2992	1.3571
05	0.15	0.1532	0.3089	-0.1876	0.3089	-0.6873	2.0065
06	0.20	0.1597	0.2797	-0.2532	0.2797	-0.8184	2.0607
07	0.15	0.0691	0.6885	0.3391	0.6885	-0.0284	2.0520
08	0.20	0.0709	0.6804	0.3335	0.6804	-0.0574	2.1270
09	0.25	0.0728	0.6715	0.3271	0.6715	-0.0779	2.1762
10	0.10	0.0984	0.5563	0.2221	0.5563	-0.1125	2.0012
11	0.15	0.1021	0.5393	0.2027	0.5393	-0.3142	2.5356
12	0.20	0.1065	0.5198	0.1790	0.5198	-0.3315	2.4981
13	0.10	0.1406	0.3657	-0.0686	0.3657	-0.3538	1.6565
14	0.15	0.1475	0.3349	-0.1316	0.3349	-0.6988	2.2160
15	0.10	0.1748	0.2116	-0.4102	0.2116	-0.4838	1.1183
16	0.15	0.0592	0.7330	0.3666	0.7330	-0.0101	2.0279
17	0.20	0.0607	0.7261	0.3627	0.7261	-0.0164	2.0429
18	0.25	0.0624	0.7184	0.3582	0.7184	-0.0207	2.0517
19	0.10	0.0843	0.6197	0.2853	0.6197	-0.0740	2.0743
20	0.15	0.0875	0.6051	0.2719	0.6051	-0.2137	2.4576

TABLE 5-2 (continued)

TEST NO.	α	ϕ	ψ'_{spth}	ψ'_{sp}	ψ'_{tpth}	ψ'_{tp}	H*
21	0.20	0.0912	0.5884	0.2558	0.5884	-0.2350	2.4758
22	0.10	0.1205	0.4563	0.0905	0.4563	-0.1782	[illegible]7346
23	0.15	0.1264	0.4299	0.0482	0.4299	-0.5026	2.4434
24	0.10	0.1498	0.3242	-0.1543	0.3242	-0.2328	1.1641
25	0.10	0.1736	0.2171	-0.3976	0.2171	-0.4637	1.1076
26	0.15	0.0518	0.7664	0.3834	0.7664	0.0038	1.9912
27	0.20	0.0531	0.7603	0.3806	0.7603	-0.0043	2.0135
28	0.25	0.0546	0.7536	0.3773	0.7536	-0.0059	2.0186
29	0.10	0.0738	0.6672	0.3240	0.6672	-0.0534	2.0994
30	0.15	0.0766	0.6545	0.3143	0.6545	-0.1191	2.2739
31	0.20	0.0798	0.6399	0.3025	0.6399	-0.1272	2.2739
32	0.10	0.1055	0.5243	0.1846	0.5243	-0.0837	1.7897
33	0.15	0.1106	0.5012	0.1549	0.5012	-0.3568	2.4777
34	0.10	0.1311	0.4087	0.0118	0.4087	-0.0959	1.2714
35	0.10	0.1519	0.3150	-0.1742	0.3150	-0.2562	1.1675
36	0.30	0.1130	0.4902	0.1400	0.4902	-0.2735	2.1807
37	0.40	0.1230	0.4452	0.0731	0.4452	-0.3110	2.0326
38	0.10	0.1818	0.1799	-0.4800	0.1799	-0.5344	1.0824
40	0.30	0.0753	0.6601	0.3187	0.6601	-0.0835	2.1775
41	0.40	0.0820	0.6301	0.2944	0.6301	-0.1177	2.2273
42	0.10	0.1212	0.4533	0.0859	0.4533	-0.1702	1.6969
43	0.20	0.1331	0.3998	-0.0041	0.3998	-0.5851	2.4385

TABLE 5-2 (continued)

TEST NO.	α	ϕ	ψ'_{spth}	ψ'_{sp}	ψ'_{tpth}	ψ'	H*
44	0.30	0.0646	0.7087	0.3523	0.7087	-0.0269	2.0638
45	0.40	0.0703	0.6830	0.3353	0.6830	-0.0413	2.0833
46	0.10	0.1039	0.5314	0.1933	0.5314	-0.1013	1.8713
47	0.20	0.1141	0.4855	0.1335	0.4855	-0.3761	2.4475
48	0.30	0.0565	0.7451	0.3730	0.7451	-0.0058	2.0181
49	0.40	0.0615	0.7226	0.3607	0.7226	-0.0168	2.0428
50	0.10	0.0909	0.5900	0.2574	0.5900	-0.0578	1.9478
51	0.20	0.0998	0.5498	0.2148	0.5498	-0.2402	2.3583

CHAPTER 6

RESULTS

HEAD-LOSS RATIO VERSUS VOID FRACTION

Having calculated H* for all the data points taken, the head-loss ratio was then plotted versus void fraction. Figure 6-1 is a plot of H* versus α with flow coefficient as a parameter, for the data taken using the plastic impeller. No sharp rise in the head-loss ratio was observed at 0.20 void fraction, as was the case for the data from the Olson experiments (reference 3-4). Rather, a gradual increase in H* with α was shown with some correlation of increasing H* with increasing flow coefficient at void fraction of $\geq$ 0.25, and flow coefficients of $\leq$ 0.13. Below a void fraction of 0.25 there was too much scatter in the data to notice any correlation of H* with ϕ_{tp}, while at flow coefficient of $\geq$ 0.13 H* tended to decrease with increasing ϕ_{tp}. The fact that the maximum value achieved for H* was less than 1.8 indicated that the plastic impeller was very inefficient in single-phase operation, and the introduction of two-phase flow did not make the performance deteriorate as greatly as it would have if the impeller had had a high single-phase efficiency.

Figure 6-2 shows the plots of ψ'_{tpth}, ψ'_{spth}, ψ'_{tp} and ψ'_{sp} versus flow coefficient for the data and geometry of the bronze impeller. Calculating H*, for appropriate values

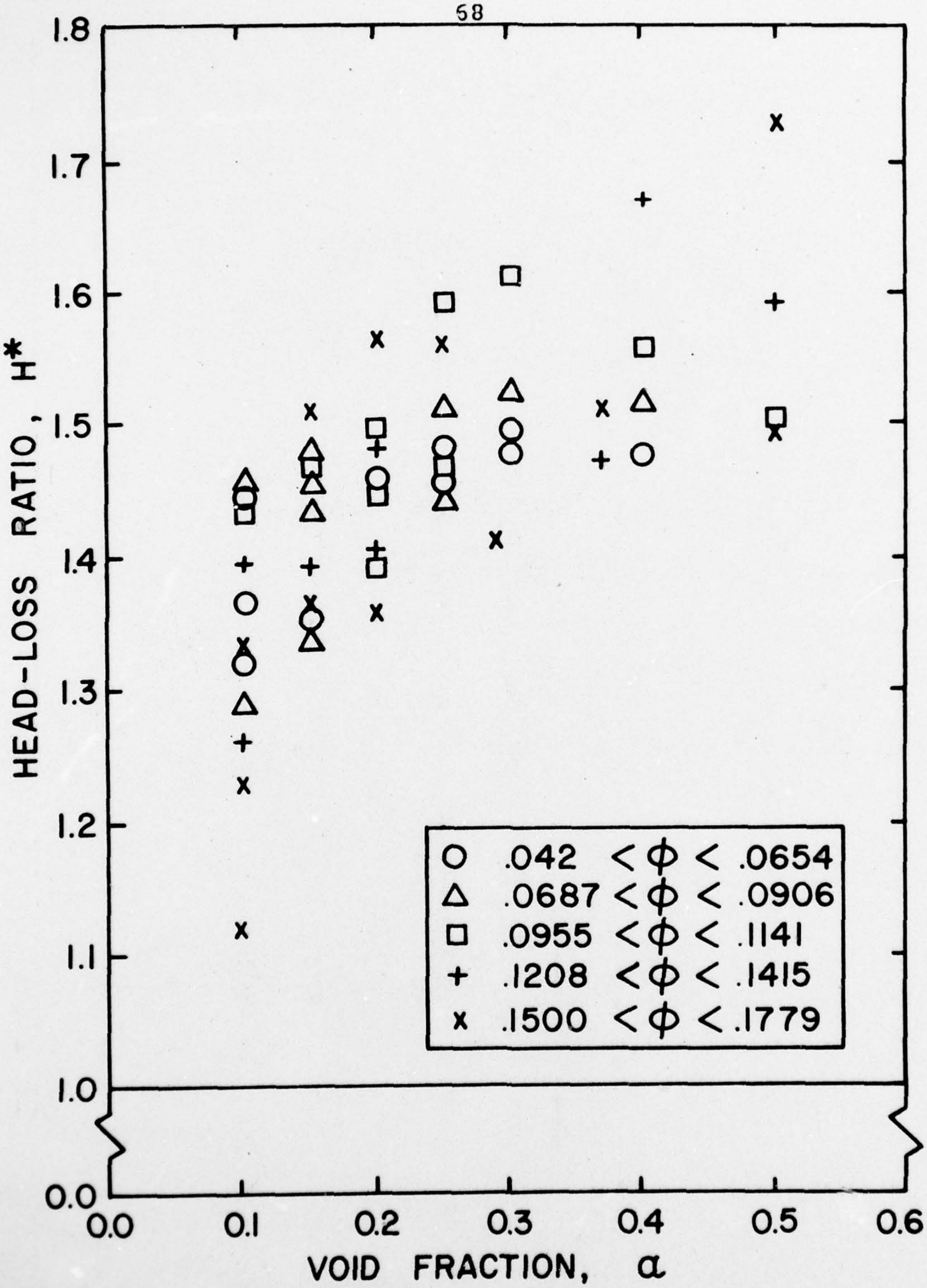

FIGURE 6-1. HEAD-LOSS RATIO VS. VOID FRACTION FOR PLASTIC-IMPELLER DATA WITH FLOW COEFFICIENT AS A PARAMETER

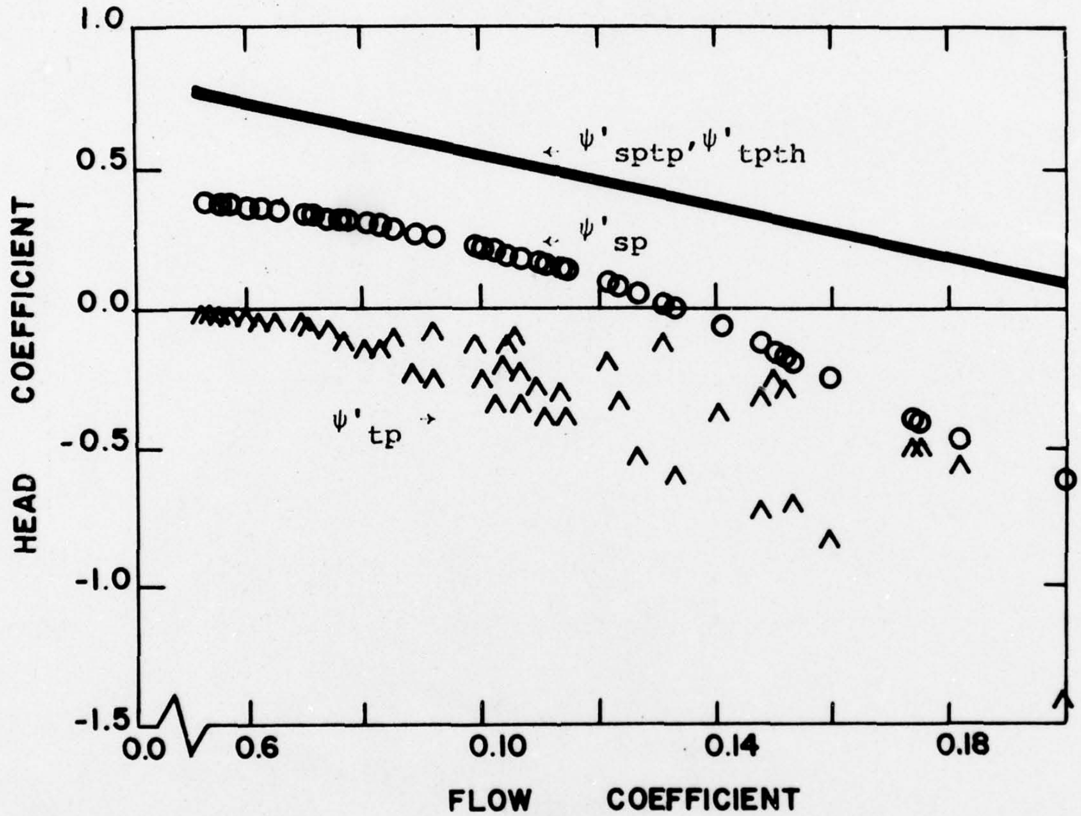

FIGURE 6-2. ACTUAL AND THEORETICAL CHARACTERISTICS OF SINGLE- AND TWO-PHASE TESTS FOR BRONZE-IMPELLER DATA

of flow coefficient, from these curves and plotting versus void fraction yielded figure 6-3. Figure 6-3 again shows a gradual increase of H* with α with no sudden jump at $\alpha = 0.20$. To better determine the existence of any possible correlation of H* with flow coefficients, plots of H* versus α for different ranges of flow coefficient were made and are given in figures 6-4 through 6-7. These plots show a better correlation of increasing H* with increasing flow coefficient than was evident from the plastic-impeller data plots. For the bronze impeller H* increased with increasing ϕ_{tp} for void fractions of ≥ 0.15, and for flow coefficients of ≤ 0.123. Above $\phi_{tp} = 0.123$ the head-loss ratio again decreased as ϕ_{tp} continued to increase. The maximum value achieved by H* for the bronze-impeller data was 2.6, indicating that the bronze impeller is more efficient in single-phase operation than is the plastic impeller, as was expected.

FLOW VISUALIZATION

Throughout the testing careful observations of the flow patterns in the inlet pipe, the impeller passages, and the scroll were made. Using the plastic impeller the major significant observation was the growth of a large air cavity in the impeller eye and its expansion across the blades into the volute as the void fraction was increased. At void fractions of 0.10 to 0.15 the impeller was covered and filled with small air bubbles recirculating through the impeller. As the

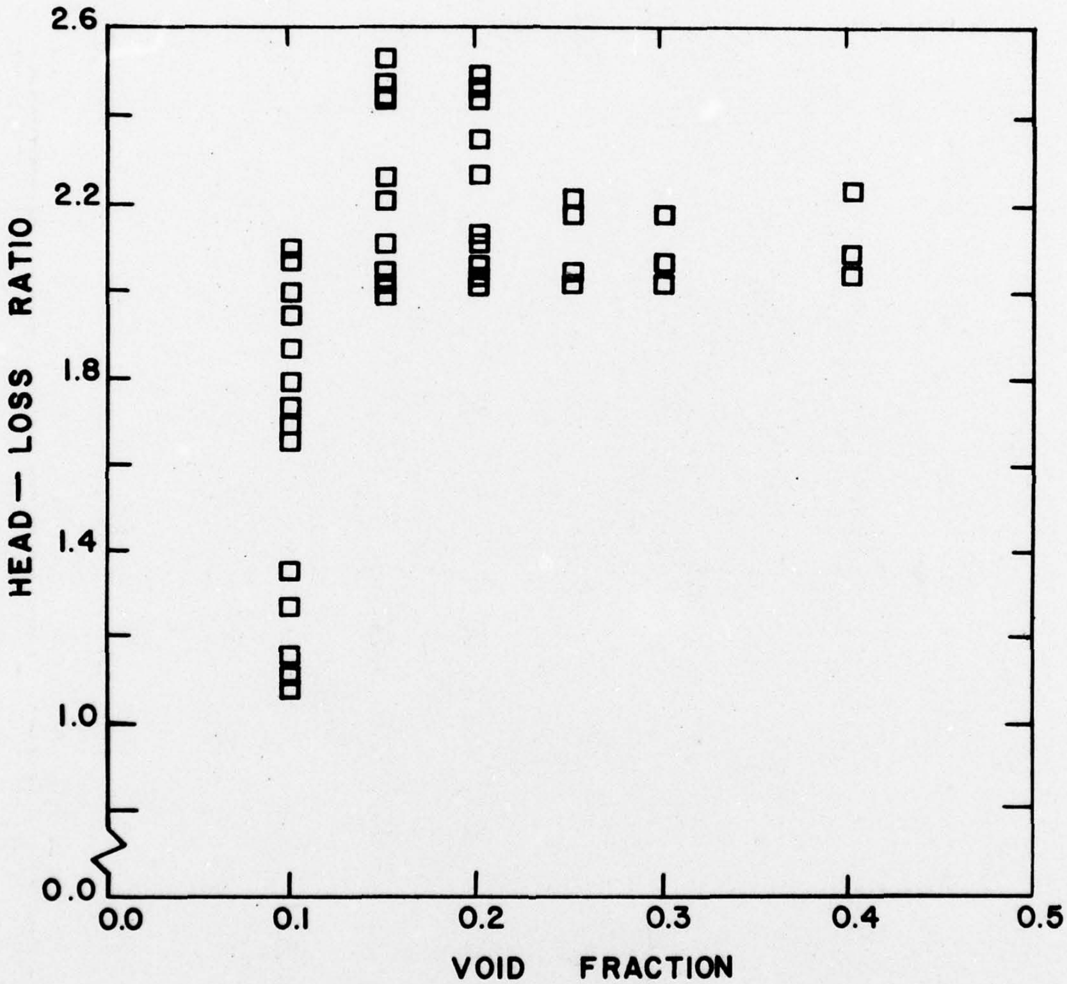

FIGURE 6-3. HEAD-LOSS RATIO VS. VOID FRACTION FOR BRONZE-IMPELLER DATA

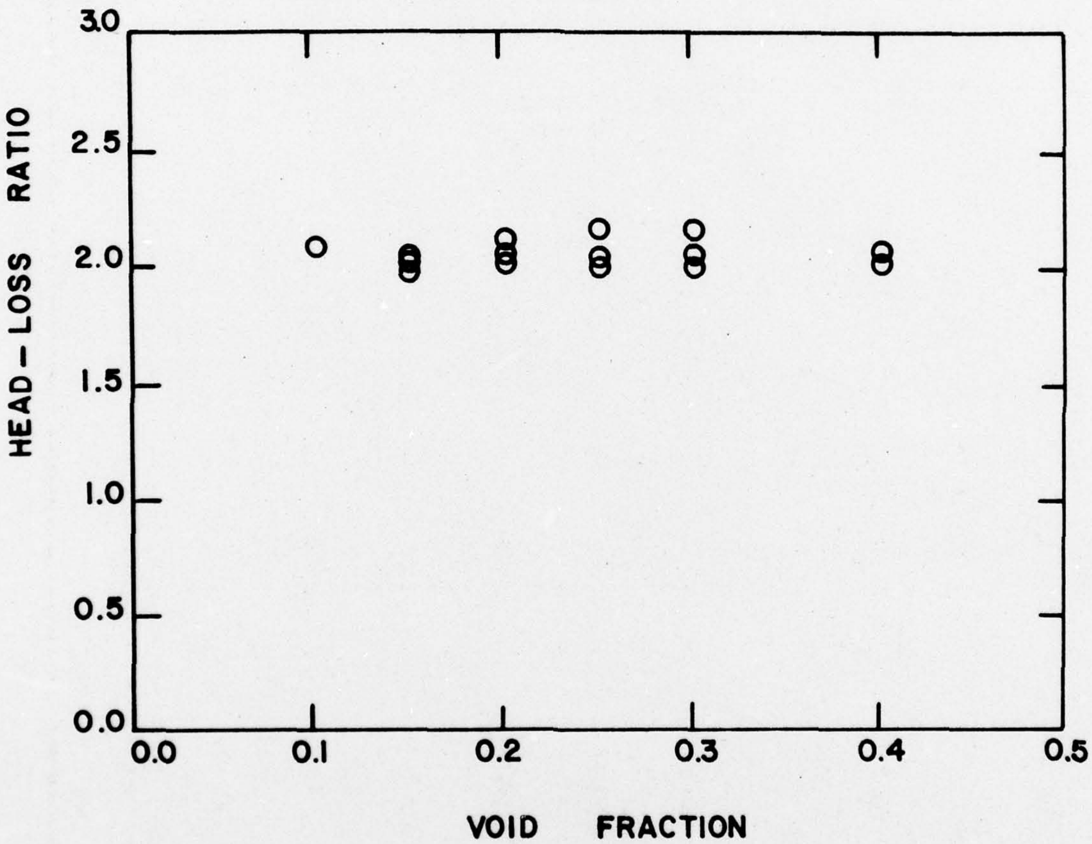

FIGURE 6-4. HEAD-LOSS RATIO VS. VOID FRACTION FOR BRONZE-IMPELLER DATA WITH $0.0 \leq \phi \leq 0.076$

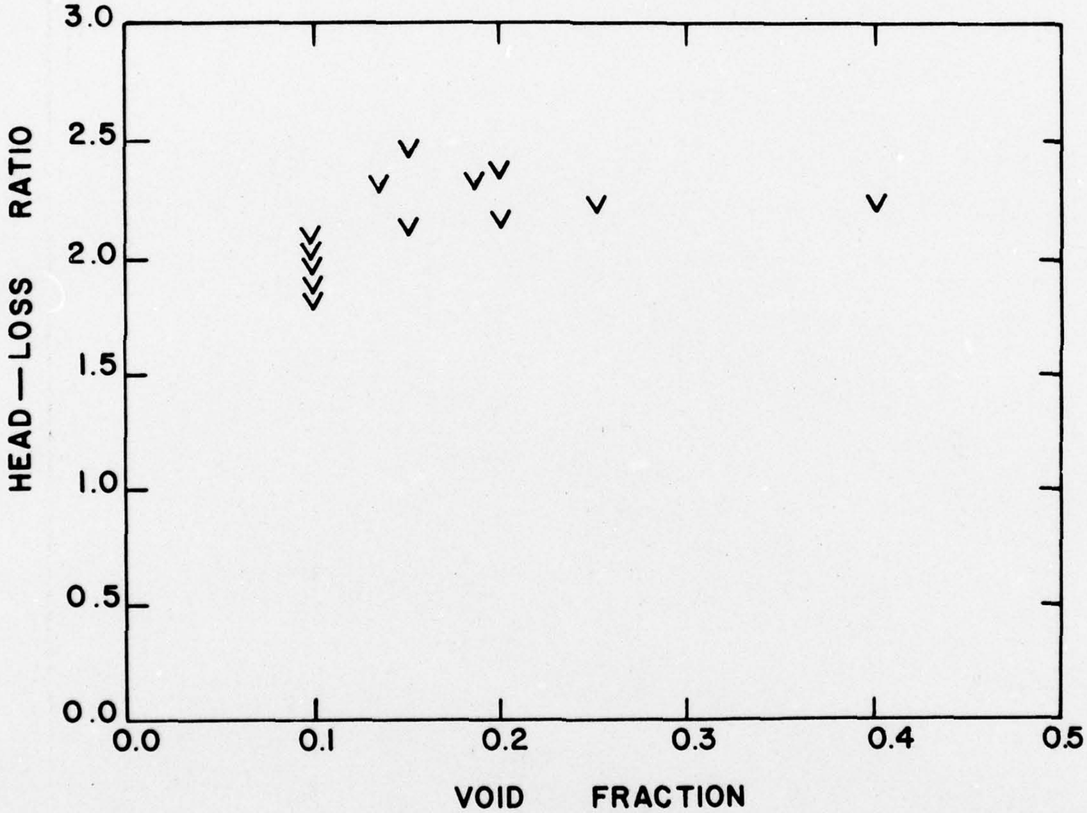

FIGURE 6-5. HEAD-LOSS RATIO VS. VOID FRACTION FOR BRONZE-IMPELLER DATA WITH $0.076 < \phi \leq 0.102$

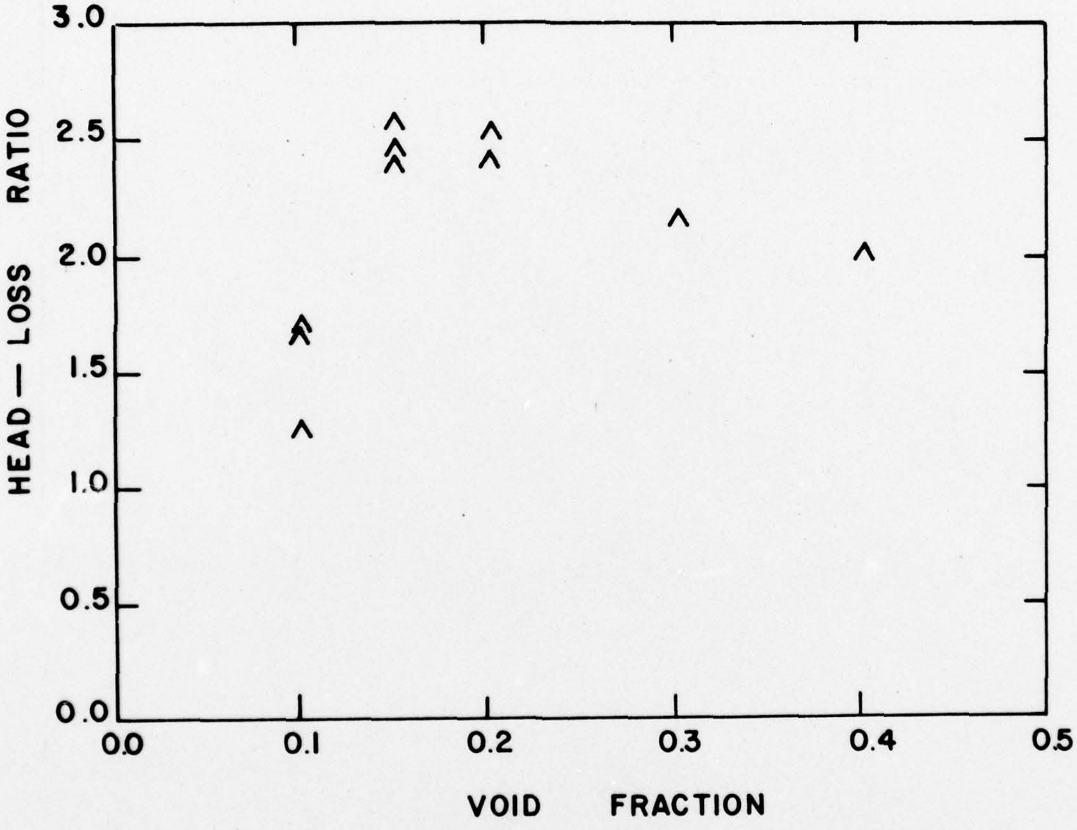

FIGURE 6-6. HEAD-LOSS RATIO VS. VOID FRACTION FOR BRONZE-IMPELLER DATA WITH $0.102 < \phi \leq 0.140$

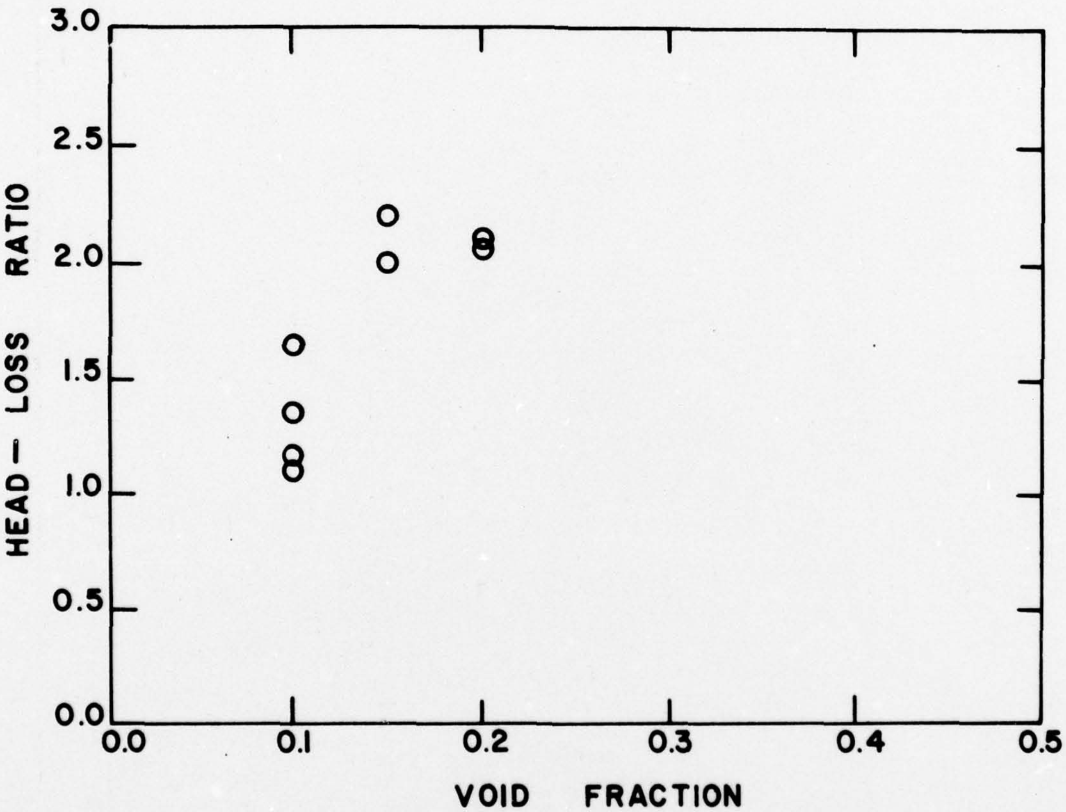

FIGURE 6-7. HEAD-LOSS RATIO VS. VOID FRACTION FOR BRONZE-IMPELLER DATA WITH ϕ > 0.140

void fraction was increased further, this air cavity in the impeller eye grew in size across the blades until at approximately $\alpha = 0.20$ the cavity had expanded out to the blade tips, with water flowing only along the bottom of the impeller. As the air cavity expanded out to the blade tips a corresponding sudden worsening of the head degradation was noticed on the static-head manometer, connected across the pump. As the void fraction increased even further, the air cavity grew into the volute with the head rise continuing to decrease, but degrading at a slower rate than that experienced while the air cavity grew to the blade tips. Once this large air cavity was formed, the inlet void fraction could be reduced to zero (single-phase water) without immediately affecting the cavity size. It took from 10 to 20 seconds for the cavity to collapse and for the pump to return to "normal" single-phase operation. In addition, this air cavity exhibited an unsteady bi-stable nature at void fractions between 0.17 and 0.20 by successively popping out to the blade tips then collapsing back into the impeller with a random frequency. Photos 6-1 through 6-4 and 6-5 through 6-8 show the growth of this air cavity from a void fraction of 0.10 to 0.40 and from 0.10 to 0.25 respectively.

The flow in the inlet pipe was also observed during the plastic-impeller tests. Determination of the void fraction from visual observations was found to be virtually

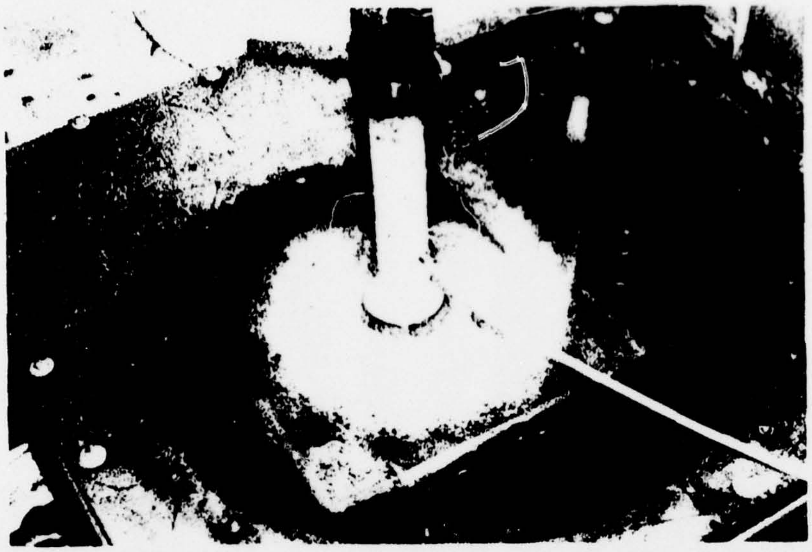

PHOTO 6-1. PLASTIC IMPELLER DURING OPERATION AT 190 RPM, $\alpha = 0.10$ AND $\phi = 0.2022$

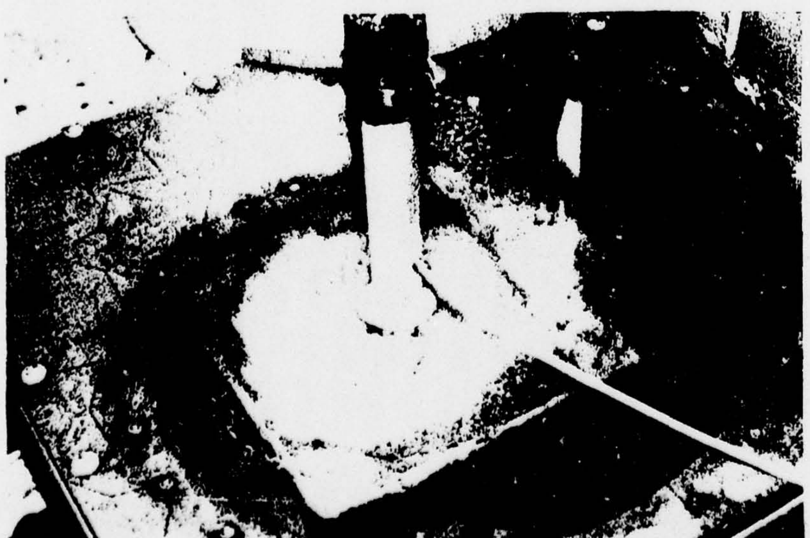

PHOTO 6-2. PLASTIC IMPELLER DURING OPERATION AT 190 RPM, $\alpha = 0.20$ AND $\phi = 0.2302$

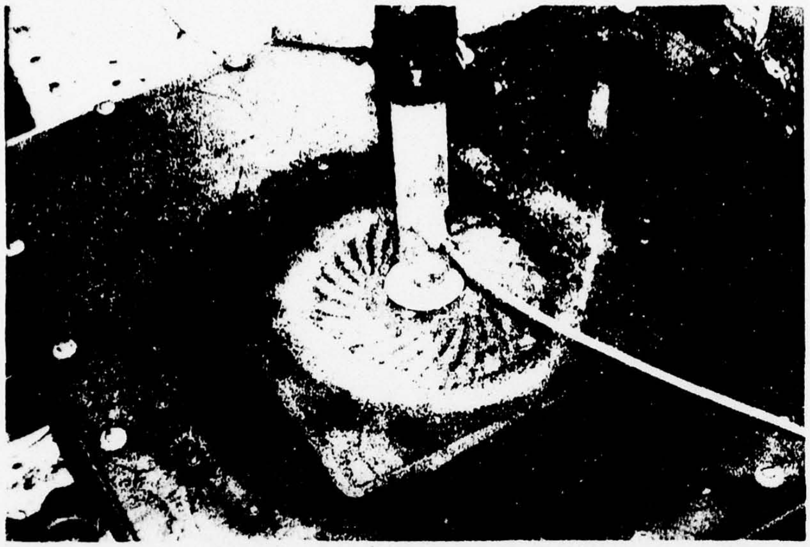

PHOTO 6-3. PLASTIC IMPELLER DURING OPERATION AT 190 RPM, $\alpha = 0.25$ AND $\phi = 0.1715$

PHOTO 6-4. PLASTIC IMPELLER DURING OPERATION AT 250 RPM, $\alpha = 0.40$ AND $\phi = 0.0598$

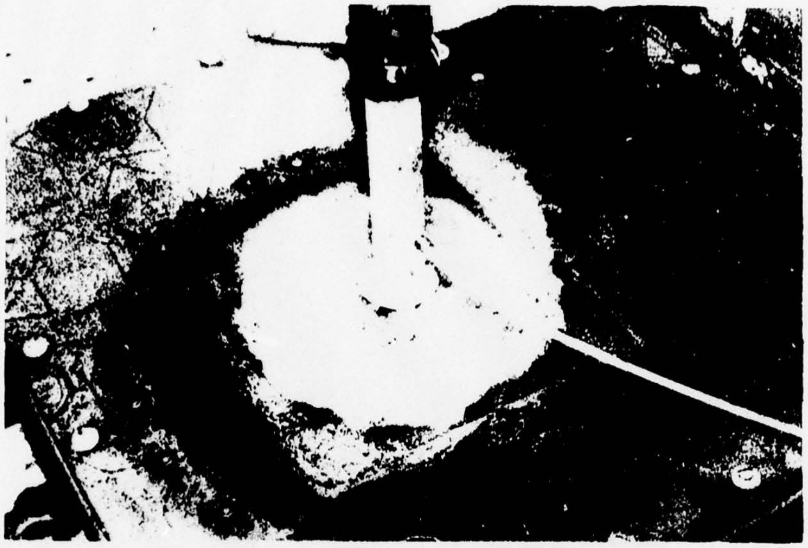

PHOTO 6-5. PLASTIC IMPELLER DURING OPERATION AT 318 RPM, $\alpha = 0.10$ AND $\phi = 0.0639$

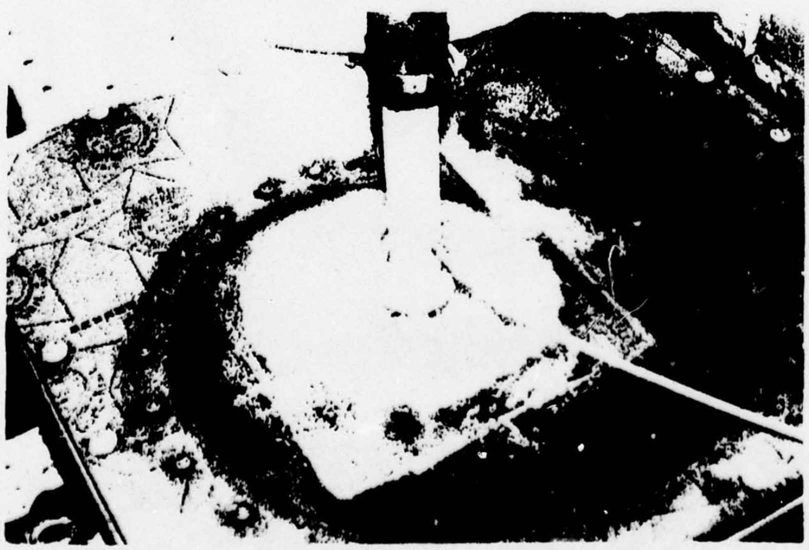

PHOTO 6-6. PLASTIC IMPELLER DURING OPERATION AT 390 RPM, $\alpha = 0.15$ NAD $\phi = 0.0731$

PHOTO 6-7. PLASTIC IMPELLER DURING OPERATION AT 390 RPM, $\alpha = 0.20$ AND $\phi = 0.0779$

PHOTO 6-8. PLASTIC IMPELLER DURING OPERATION AT 390 RPM, $\alpha = 0.25$ AND $\phi = 0.0835$

impossible, although a pulsing slug-flow was seen to develop at a void fraction of 0.20 - 0.25.

Since the bronze impeller was shrouded no observations of the flow within the blade channels was possible. However, the flow in the inlet pipe, at the blade tips, and in the volute was carefully noted. Photos 6-9 through 6-12 show the inlet-pipe flow during void fractions of 0.10 to 0.40. For void fractions of 0.10 - 0.20 the inlet flow was filled with dispersed bubbles traveling down the pipe with the water flow. However, at void fraction of $\geq$ 0.20 the bubbles became more mixed and, in various sections of the pipe, reversed their downward flow direction. As the void fraction was increased from 0.20 to 0.40 this flow reversal became stronger and a pulsing slug-flow developed.

No expanding air cavity was noticed at the blade tips or in the scroll during the bronze-impeller tests. Throughout the range of void fraction the impeller periphery was surrounded with small air bubbles. The size of these bubbles increased with a decrease in the pump rotational speed and as the bubbles flowed from the narrower to the wider scroll area. In addition, a stagnant water and air void filled from one-quarter to one-half of the scroll exit area adjacent to the cutwater throughout the two-phase testing. Typical flow configurations at the blade tips and in the scroll are shown in photos 6-13 through 6-20.

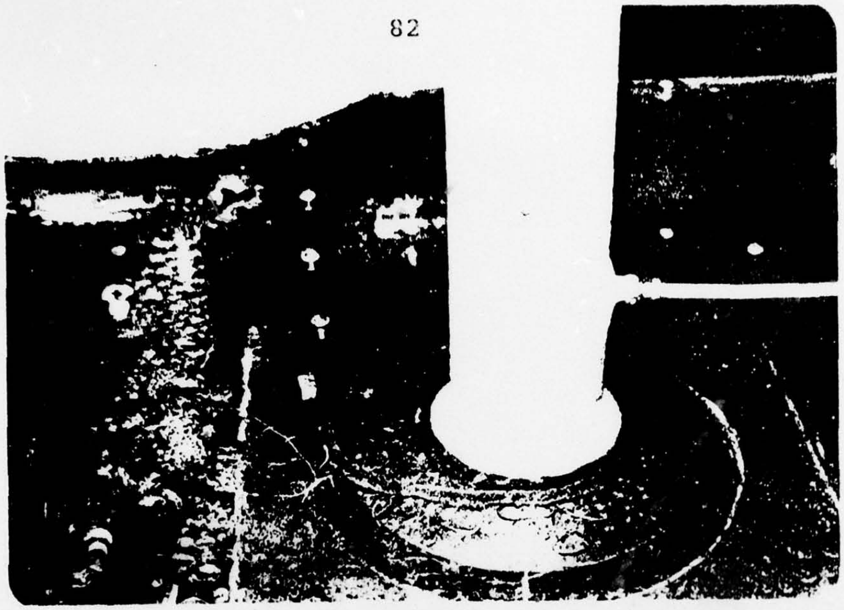

PHOTO 6-9. INLET-PIPE FLOW FOR 200 RPM, α = 0.10 AND ϕ = 0.1476

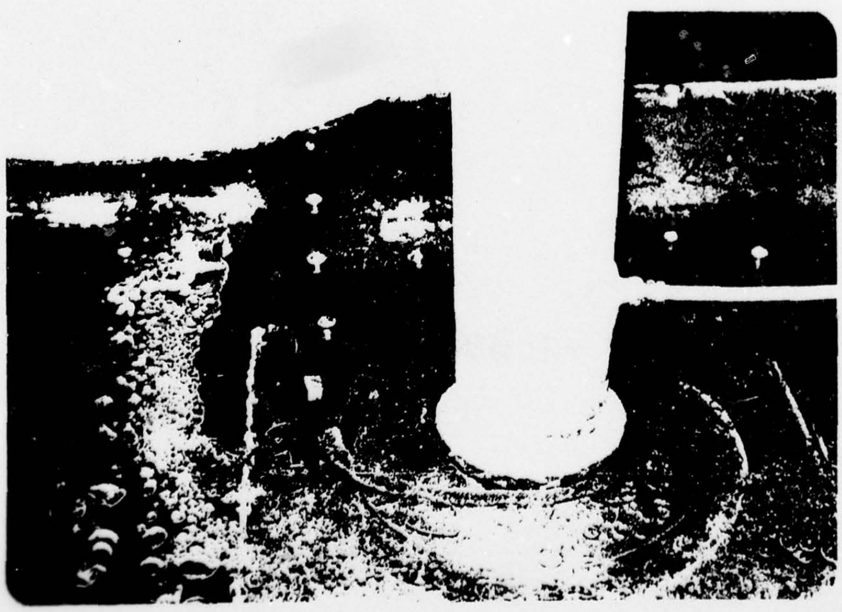

PHOTO 6-10. INLET-PIPE FLOW FOR 200 RPM, α = 0.15 AND ϕ = 0.1532

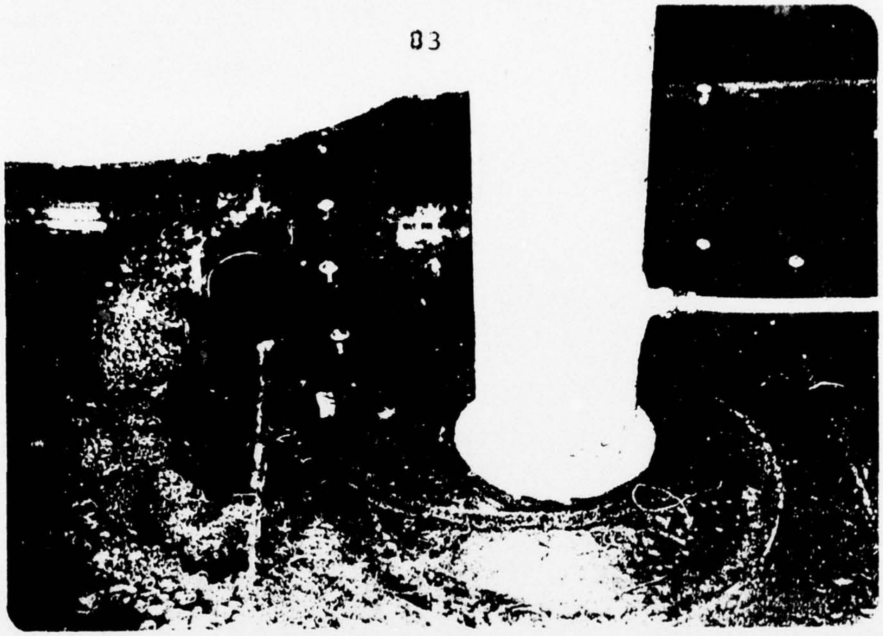

PHOTO 6-11. INLET-PIPE FLOW FOR 200 RPM, α = 0.20 AND ϕ = 0.1597

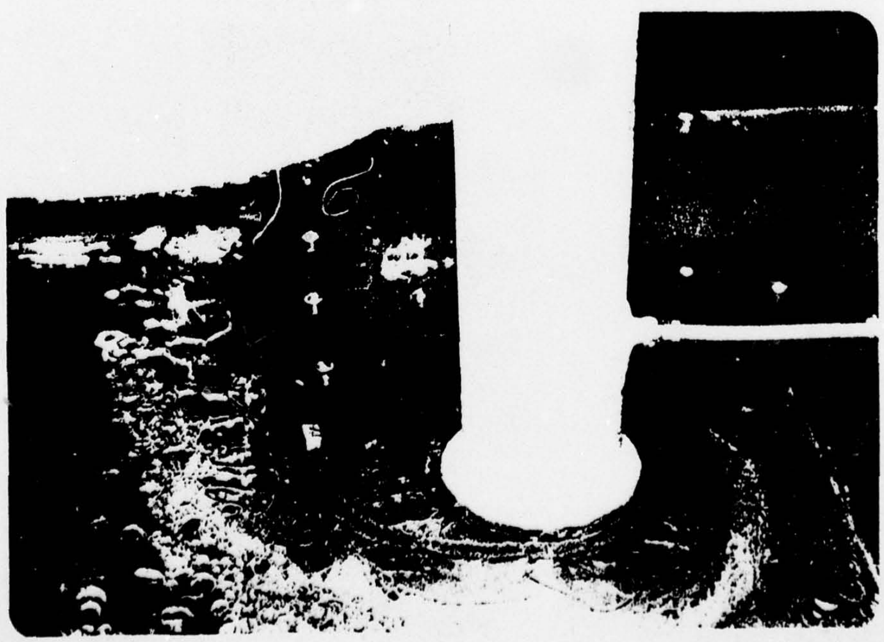

PHOTO 6-12. INLET-PIPE FLOW FOR 200 RPM, α = 0.40 AND ϕ = 0.1230

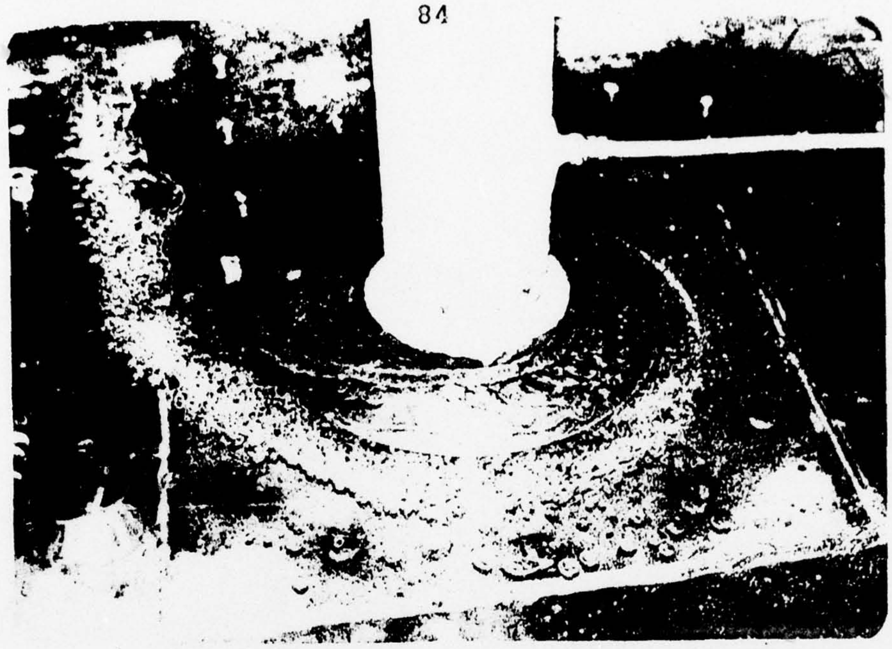

PHOTO 6-13. BRONZE IMPELLER DURING OPERATION AT 200 RPM, $\alpha = 0.10$ AND $\phi = 0.1476$

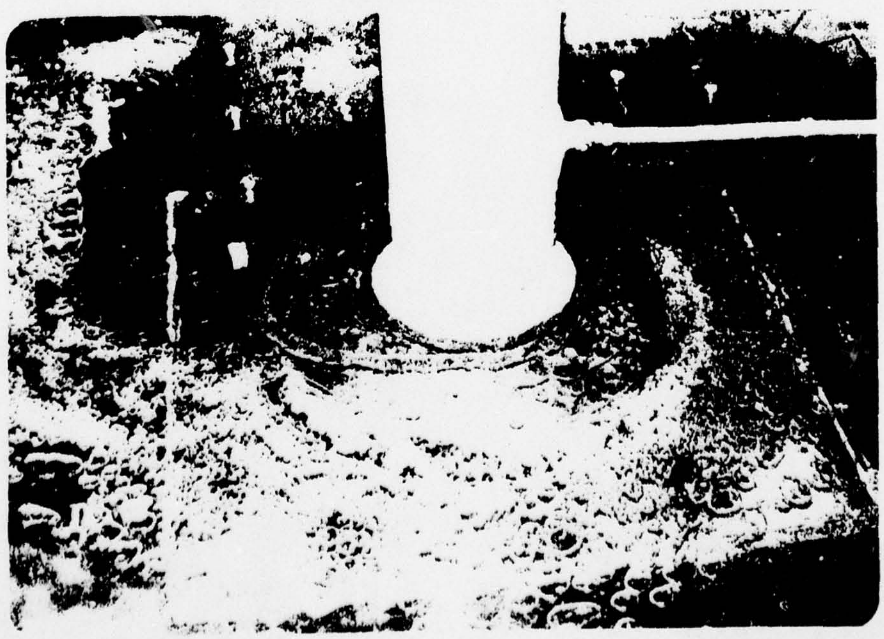

PHOTO 6-14. BRONZE IMPELLER DURING OPERATION AT 200 RPM, $\alpha = 0.20$ AND $\phi = 0.1597$

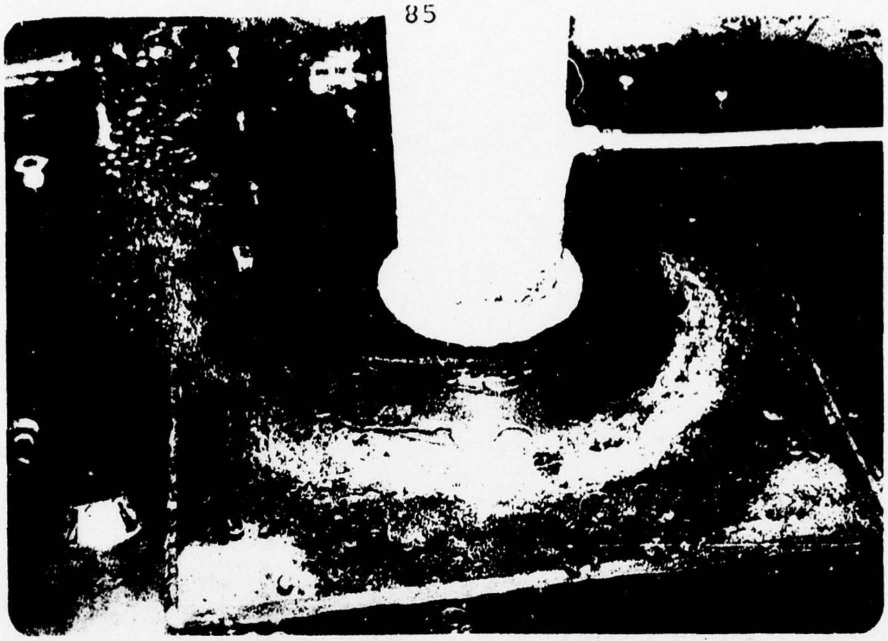

PHOTO 6-15. BRONZE IMPELLER DURING OPERATION AT 400 RPM, $\alpha = 0.10$ AND $\phi = 0.0738$

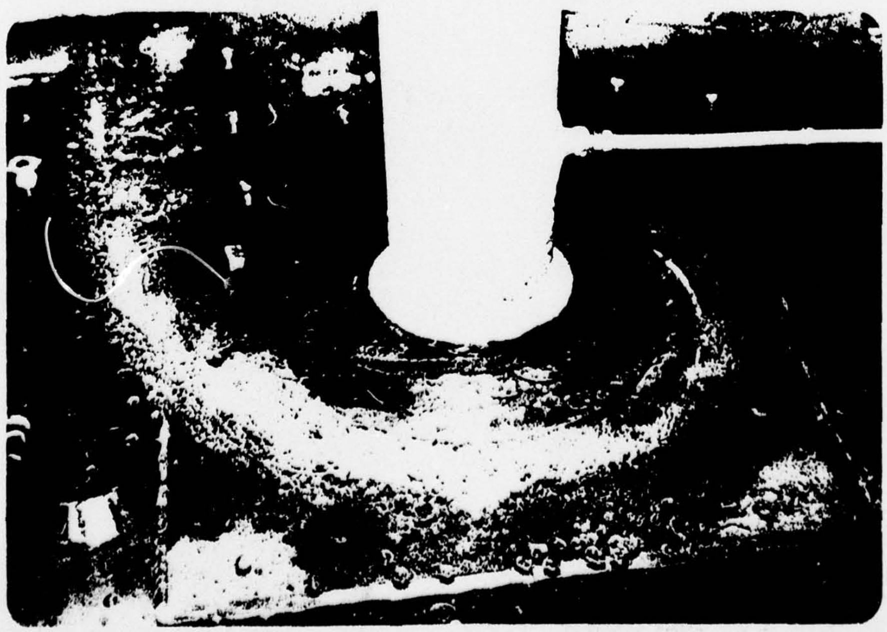

PHOTO 6-16. BRONZE IMPELLER DURING OPERATION AT 400 RPM, $\alpha = 0.20$ AND $\phi = 0.0799$

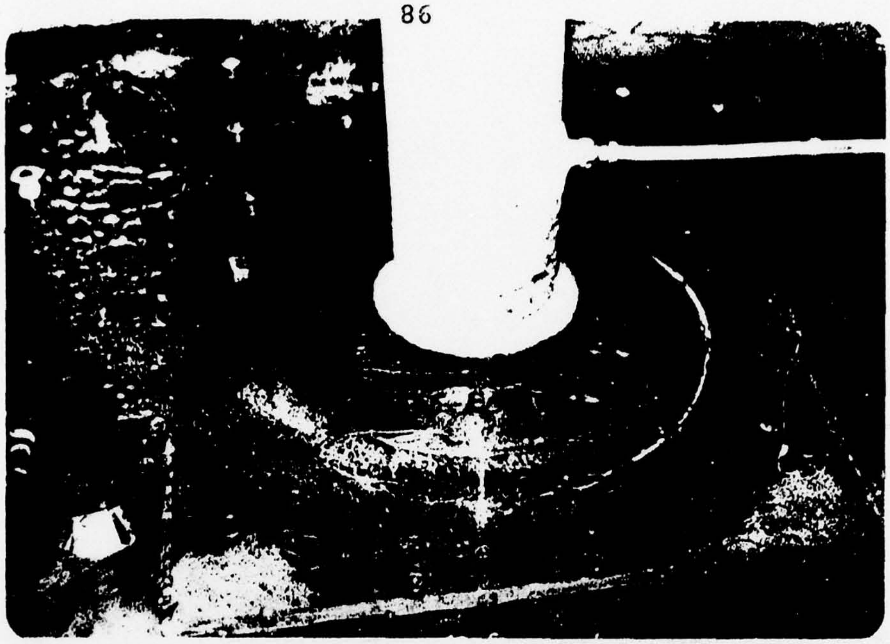

PHOTO 6-17. BRONZE IMPELLER DURING OPERATION AT 200 RPM, $\alpha = 0.30$ AND $\phi = 0.1131$

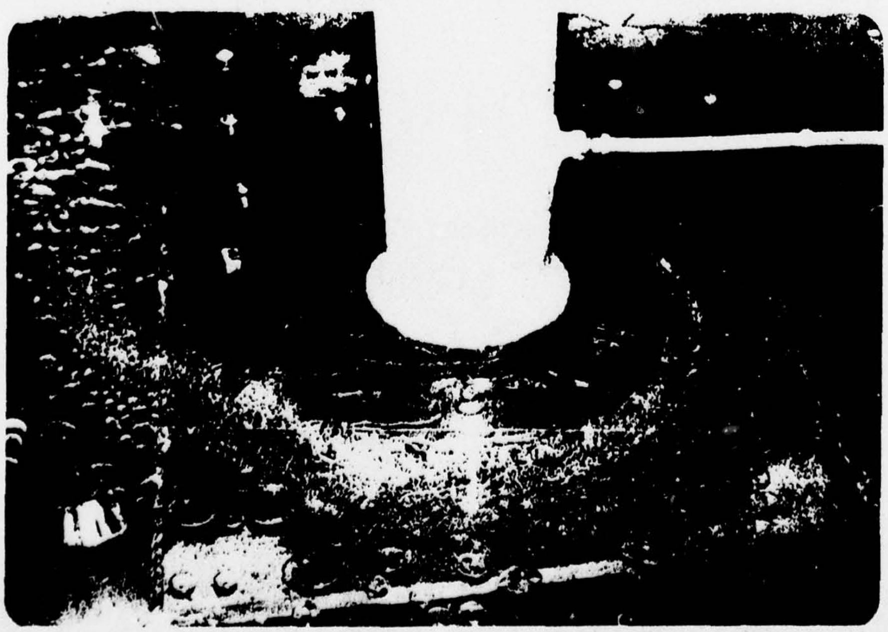

PHOTO 6-18. BRONZE IMPELLER DURING OPERATION AT 200 RPM, $\alpha = 0.40$ AND $\phi = 0.1230$

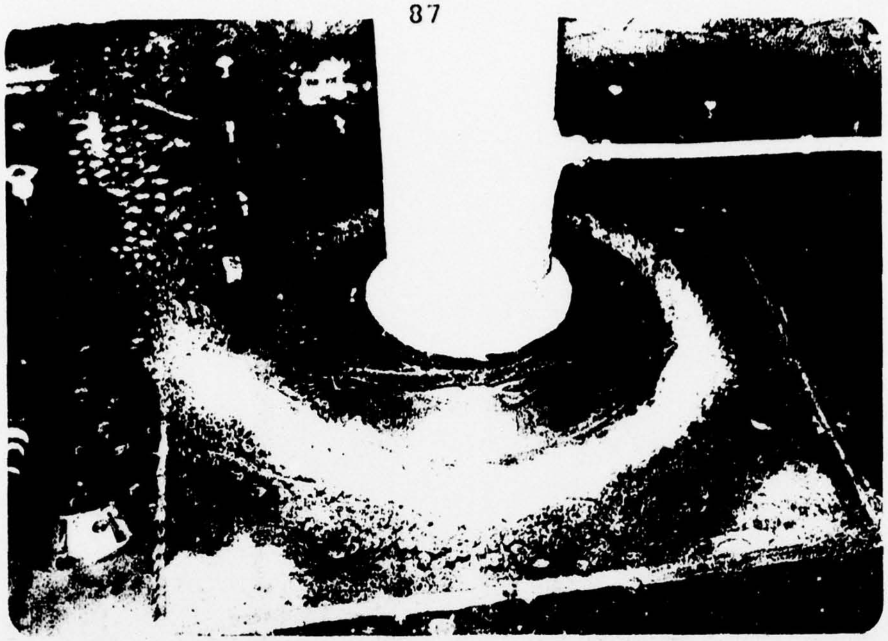

PHOTO 6-19. BRONZE IMPELLER DURING OPERATION AT 400 RPM, $\alpha = 0.30$ AND $\phi = 0.0565$

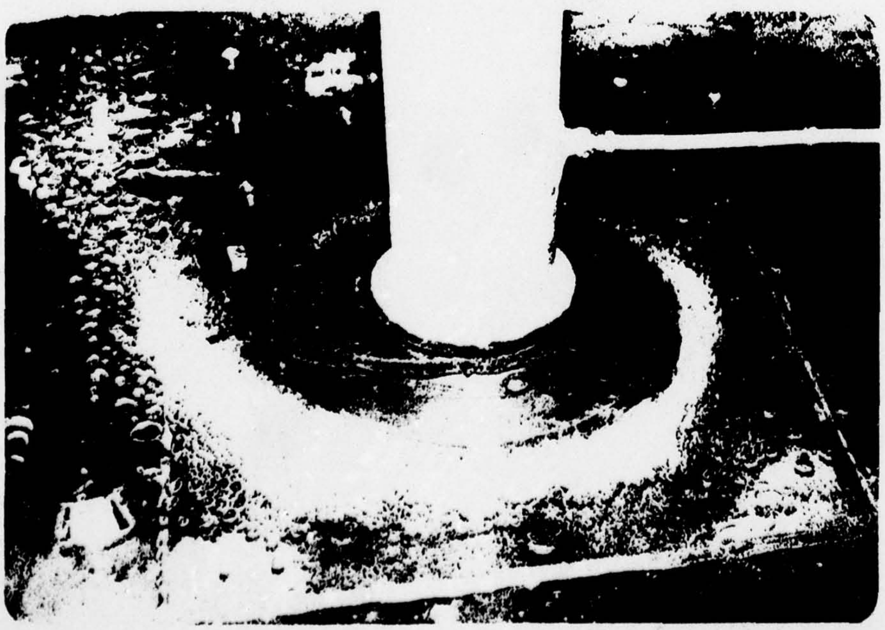

PHOTO 6-20. BRONZE IMPELLER DURING OPERATION AT 400 RPM, $\alpha = 0.40$ AND $\phi = 0.0615$

CHAPTER 7

CONCLUSIONS

The most significant conclusion drawn from these experiments is the correlation of H* with flow coefficient as well as with void fraction. Although this correlation is visible only for $\alpha \geq 0.25$ in the plastic-impeller data, the data for the bronze impeller show a much stronger correlation for $\alpha \geq 0.15$. The lack of any definite correlation between H* and flow coefficient at the lower void fractions may be due to two possibilities. First of all, the flow regime of the inlet flow for $0.10 \leq \alpha \leq 0.20$ may be continually changing from dispersed bubble to elongated bubble to slug-flow and back again with no apparent regularity. Also, for low void fractions at flow coefficients below design point, H* increases with increasing ϕ_{tp}. However, for low void fractions at flow coefficients greater than design point the single-phase head losses increase with flow coefficient at a faster rate than the two-phase losses, causing H* to decrease with increasing ϕ_{tp}. Thus, the randomness of the correlation between H* and flow coefficient at low void fractions could be explainable. For higher void fractions the correlation shows two separate trends. For flow coefficients between 0.0 and the single-phase design point (minimum single-phase losses), the head-loss ratio increases with increasing

ϕ_{tp}. The reason for this is that the single-phase losses decrease while the two-phase losses increase, as the flow coefficient increases toward design point. However, as the flow coefficient increases past design point the single-phase losses increase at a faster rate than the two-phase losses, casuing H* to decrease with increasing flow coefficient.

The flow-visualization tests also led to some significant conclusions. The blanketing of the plastic impeller with an air cavity at $\alpha \geq 0.20$ and the subsequent drastic head degradation shows that the flow regime inside the impeller affects pump performance to a great degree. In addition, the flow regime inside the impeller could not be determined from the inlet or outlet flow regimes. This phenomenon may well be the cause of "unsteady" steady-state data and inconsistent data readings (reference 7-1). It was also noted that for the same air- and water-flow rates, as rpm was increased (decreasing ϕ_{tp}) the air cavity took longer to form. It appears that the high rotational speeds cause the inlet bubbles to be chopped into smaller bubbles by the blades, and thereby delay the formation of the large air cavity. The absence of the air cavity in the bronze-impeller tests seems to support this trend of thought. Unlike the plastic impeller, the bronze impeller had blades which curved upward into the impeller inlet. This blade configuration is more capable of chopping up the inlet flow

than that of the flat plastic impeller. Consequently, throughout the range of void fractions tested, the blade tips were surrounded by small air bubbles, decreasing in size as the rotational speed was increased (decreasing flow coefficient), rather than being blanketed by an air cavity.

The flow-visualization studies also indicate that the location of the cutwater significantly affects the flow pattern in the volute. During the two-phase tests using the bronze impeller the cutwater created a stagnant water and air void, filling between one-quarter and one-half of the exit scroll area. Depending upon the location of the pressure taps in the exit scroll, such a flow pattern can greatly affect the validity of the head readings across the pump.

Finally, the importance of accurately determining the slip-factor should be noted. The value of the relative outlet angle, determined from the slip-factor correlation, is vital in determining the theoretical characteristic curves. For these experiments β_2 was determined for a particular operating-point flow coefficient and was used as a constant throughout the tests. It is generally recognized that β_2 varies with void fraction and flow coefficient, although no direct correlation is available at the time.

CHAPTER 8

RECOMMENDATIONS

A number of options are available for improving upon the results of this experiment. First of all, I believe interesting results could be obtained by machining off the shroud of the bronze impeller so that the flow through the blade passages could be observed. In addition, as a later modification the scroll and cutwater should be redesigned for optimum first-quadrant operation of the bronze impeller. Tests could then be run at speeds of approximately 1700 rev/min and for void fractions of 0 to 1.0. This would provide a more complete and comprehensive data base and also provide the opportunity to observe the flow within the impeller passages for the complete range of flow conditions. The results from such a program should be able to define more clearly the correlation of H* with void fraction, flow coefficient, and, possibly, other applicable parameters. Specifically, specific-speed is one such parameter which should be investigated to determine its effect, if any, on the head-loss ratio. Finally, a high-speed-strobe photographic study of the deviation angle, δ, at the blade tips could be done by injecting dye into the flow or attaching directional threads to the blade tips. Such a study could provide more information on the change in δ with void fraction

and flow coefficient.

APPENDIX A

THE BUSEMANN SLIP FACTOR

The Busemann slip factor, σ_B, is defined as the ratio of the blade-tip tangential components of the absolute velocity corresponding to the relative outlet-flow angle, β_2, and the blade outlet angle, β_2'. Busemann's theory applies to two-dimensional vanes curved as logarithmic spirals (blade angle β' is constant for all radii). Mathematically, the Busemann slip factor can be written as

$$\sigma_B = (A-B\phi_2 \tan(90°-\beta_2'))/(1-\phi_2 \tan(90°-\beta_2')) \qquad \text{(A-1)}$$

where A and B are functions of r_2/r_1, β_2', and Z. Specifically, B = 1.0 and is constant for all conditions if

$$\frac{r_2}{r_1} \geq \exp((2\pi\cos(90°-\beta'))/Z)$$

This criterion can also be applied to other than logarithmic-spiral vanes if β_2' is used instead of β'. Applying this criterion to the plastic and bronze impellers yielded the following results:

Plastic Impeller

$\beta_2' = 46°$

$Z = 24$

$r_2 = 4\ 3/32$ inches

$r_1 = 2\ 1/8$ inches

$$\frac{r_2}{r_1} = 1.926 \overset{?}{\geq} \exp[(2\pi\cos 44°)/24]$$

$1.926 > 1.207$

Therefore, B = 1.0

Bronze Impeller

$\beta_2' = 25°$

$Z = 5$

$r_2 = 3\ 21/32$ inches

$r_1 = 1\ 13/32$ inches

$$\frac{r_2}{r_1} = 2.60 \overset{?}{\geq} \exp[(2\pi\cos 65°)/5]$$

$2.60 > 1.70$

Therefore, $B = 1.0$

Similarly, the value of A depends on β_2' and Z only and was found to equal 0.92 and 0.76 for the plastic and bronze impellers respectively (reference A-1). Substituting these values and the appropriate flow coefficients into equation A-1 yielded the following results:

Plastic Impeller

$$\sigma_B = \frac{0.92 - (1.0)(0.5178)\tan 44°}{1 - 0.5178\tan 44°} = 0.84 = \frac{C_{\phi 2}}{C'_{\phi 2}}$$

Bronze Impeller

$$\sigma_B = \frac{0.76 - (1.0)(0.03434)\tan 65°}{1 - 0.03434\tan 65°} = 0.741 = \frac{C_{\phi 2}}{C'_{\phi 2}}$$

From these ratios and the information contained in the outlet velocity triangles, relative outlet flow angles of 41.76° and 12.5° were obtained for the plastic and bronze impellers respectively.

APPENDIX B

DETERMINATION OF THE SCROLL CONFIGURATION

Since no performance data on the plastic impeller were available, the first step in determining the scroll configuration was to assume a ϕ_{be}. Using Busemann's slip-factor correlation, the geometry of the plastic impeller and $\phi_{be} = 0.5178$, the relative outlet-flow angle, β_2, was found to be 41.76° (reference 1) (see Appendix A). From the geometry of the blade-outlet velocity triangle (see figure 4-1), and employing the above values of ϕ_{be}, β_2 and the definition of flow coefficient, $\phi \equiv \frac{C_m}{u}$, the following relations were arrived at.

$$\phi_2 \equiv \frac{C_{m2}}{u_2} = 0.5178 \text{ or } C_{m2} = 0.5178u_2$$

$$C_2 = \frac{C_{m2}}{\cos 39.05°} = 0.6667u_2$$

Now, the scroll was designed to maintain the value of C_2 throughout the scroll. Since the total-outlet area through which C_{m2} flowed was measured to be 6 square inches, the total-outlet area through which C_2 flowed was (6 in^2)cos 39.05°, or 4.66 in^2. Since the plastic impeller had 24 exit channels, the area in each channel through which C_2 flowed was $\frac{4.66 \text{ in}^2}{24} = 0.1942 \text{ in}^2$.

AD-A052 638 MASSACHUSETTS INST OF TECH CAMBRIDGE DEPT OF ELECTRI--ETC F/G 20/4
FIRST-QUADRANT TWO-PHASE FLOW IN CENTRIFUGAL PUMPS.(U)
JAN 77 R D ZEGLEY

UNCLASSIFIED NL

2 OF 2
AD
A052638

END
DATE
FILMED
5-78
DDC

Thus, for C_2 to be maintained throughout the exit scroll the scroll area must increase 0.1942 in^2 every 15° of arc. Since the blade and scroll channels were both 0.5 inches deep, the scroll was designed to increase

$$\frac{0.1942\ in^2}{0.5\ in} = 0.388 \text{ inches in radius for every } 15° \text{ of arc.}$$

APPENDIX C

CALCULATION OF TWO-PHASE DYNAMIC HEAD

The two-phase dynamic head across the pump is equal to the sum of the liquid- and vapor-phase dynamic heads.

$$\Delta p_{dyn\ tp} = \left[\frac{\rho_{L2}C_{L2}^2}{2g_c} + \frac{\rho_{v2}C_{v2}^2}{2g_c}\right] - \left[\frac{\rho_{L1}C_{L1}^2}{2g_c} + \frac{\rho_{v1}C_{v1}^2}{2g_c}\right]$$

$$\frac{\Delta p_{dyn\ tp}}{\rho_{tp}} = \Delta H_{dyn\ tp} = \left[\frac{\rho_{L2}C_{L2}^2}{2g_c\rho_{tp}} + \frac{\rho_{v2}C_{v2}^2}{2g_c\rho_{tp}}\right] - \left[\frac{\rho_{L1}C_{L1}^2}{2g_c\rho_{tp}} + \frac{\rho_{v1}C_{v1}^2}{2g_c\rho_{tp}}\right]$$

where

$$\rho_{tp} \equiv \frac{\rho_v s\alpha + (1-\alpha)\rho_L}{(1-\alpha) + s\alpha} \;; \qquad s \equiv \frac{J_v(1-\alpha)}{J_L\alpha}$$

Therefore,

$$\Delta H_{dyn\ tp} = \left[\frac{\rho_{L2}\left(\frac{Q_{L2}}{A_{L2}}\right)^2}{2g_c\rho_{tp}} + \frac{\rho_{v2}\left(\frac{Q_{v2}}{A_{v2}}\right)^2}{2g_c\rho_{tp}}\right] - \left[\frac{\rho_{L1}\left(\frac{Q_{L1}}{A_{L1}}\right)^2}{2g_c\rho_{tp}} + \frac{\rho_{v1}\left(\frac{Q_{v1}}{A_{v1}}\right)^2}{2g_c\rho_{tp}}\right]$$

However,

$$\alpha \equiv \frac{A_v}{A_T} \;; \quad 1 - \alpha = \frac{A_L}{A_T}$$

Resulting in

$$\Delta H_{dyn\ tp} = \left[\frac{\rho_{L2}\left(\frac{Q_{L2}}{(1-\alpha)A_{T2}}\right)^2}{2g_c\rho_{tp}} + \frac{\rho_{v2}\left(\frac{Q_{v2}}{\alpha A_{T2}}\right)^2}{2g_c\rho_{tp}}\right] -$$

$$\left[\frac{\rho_{L1}\left(\frac{Q_{L1}}{(1-\alpha)A_{T1}}\right)^2}{2g_{c\ tp}\rho} + \frac{\rho_{v1}\left(\frac{Q_{v1}}{\alpha A_{T1}}\right)^2}{2g_c\rho_{tp}}\right]$$

In performing the two-phase dynamic-head calculations it was discovered that the contribution of the vapor-phase was negligible, and was, therefore, neglected for subsequent calculations.

APPENDIX D

THE DRIFT-FLUX MODEL

The drift-flux model, developed by Zuber and Wallis, satisfactorily accounts for the influcence of mass velocity on the void fraction and is useful in the bubbly-, slug-, and churn-flow regimes (reference 3-2). The details of the drift-flux model are given below.

$$\alpha = \left[\frac{J_V}{1.2(J_L+J_V) \pm 0.35(gd)^{1/2}}\right] \quad \begin{matrix} + = \text{upflow} \\ - = \text{downflow} \end{matrix} \qquad \text{(D-1)}$$

$$J_V \equiv \text{superficial vapor velocity} \equiv \frac{\dot{m}_V}{\rho_V A_T} = \frac{Q_V}{A_T}$$

$$J_L \equiv \text{superficial liquid velocity} \equiv \frac{\dot{m}_L}{\rho_L A_T} = \frac{Q_L}{A_T}$$

$d \equiv$ inlet-pipe diameter

Substituting for J_V and J_L, equation D-1 becomes

$$\alpha = \left[\frac{Q_V}{1.2(Q_V+Q_L) - (0.35)(gd)^{1/2}A_T}\right] \qquad \text{(D-2)}$$

After some mathematical manipulation equation C-2 can be transformed to

$$Q_V = \frac{1.2\alpha Q_L - 0.35(gd)^{1/2}A_T}{(1 - 1.2\alpha)} \qquad \text{(D-3)}$$

Thus, for a desired void fraction and water-flow rate an appropriate air-flow rate was calculated using equation D-3.

APPENDIX E

COMPUTER PROGRAMS

CALCULATION OF TWO-PHASE DYNAMIC HEAD

```
0004R          DENWAT = 62.4
000CR          AREA = 0.0581
0014R          ND = 51
001CR          CF = 539.44
0024R          WRITE (5,8)
0038R     8    FORMAT (1H1, 5X,'      TEST NO.      ', 5X, '     FLOW COEFFICIENT
0038R         1 ',5X, ' VOID FRACTION  ', 5X, 'DYNAMIC HEAD    ', 3X,'TWO-PHASE
0038R         2DENSITY')
00BER          DO 5 I = 1,ND
00C6R          READ (8,6) NUM, QWAT, QAIR, N, PRESS, VOID
010AR     6    FORMAT (I10, 2F12.5, I10, 2F12.4)
0128R          QTOT = QWAT + QAIR
0134R          FCOEFF = (QTOT/FLOAT(N)) * CF
014CR          DENAIR = (PRESS+14.7) *144. /(53.34 * 530.)
0170R          SPAIR = QAIR / AREA
017CR          SPWAT = QWAT / AREA
0188R          SLIP = SPAIR * (1.-VOID) / (SPWAT * VOID)
01ACR          TPDEN = (DENAIR*VOID*SLIP +(1.-VOID) * DENWAT)
01ACR         1 /(1.-VOID + SLIP * VOID)
01F4R          DYNHD = (1076.8305*QWAT**2)/(TPDEN*(1.-VOID)**2)
0228R          WRITE (5,10) NUM, FCOEFF, VOID, DYNHD, TPDEN
0264R    10    FORMAT ( 5X, I10, 4(F17.5,5X), /)
0280R     5    CONTINUE
0290R          END
```

SINGLE-PHASE DATA CURVE-FIT

```
0004R          DIMENSION PLOT (3,30)
0004R          DIMENSION  FLCOEF(30), HSP(30),              CHECK (30), PERCEN(30)
0004R           DIMENSION  COEFF(7)
0004R          ND = 29
000CR          AND = 29.
0014R          NCEF = 7
001CR          DO 5 I= 1, ND
0024R          READ (8,6) FLCOEF(I),HSP(I)
0078R          PLOT (1,I) = FLCOEF(I)
00AAR           PLOT (2,I) = HSP(I)
00DCR        6 FORMAT (2F12.5)
00EAR     5    CONTINUE
00FAR          CALL LSFIT (ND, NCEF, FLCOFF, HSP, COEFF)
010AR          WRITE (5,9) COEFF
0128R     9    FORMAT (//, '  THE COEFFICIENTS ARE :    ', 7E13.5)
0158R          WRITE (5,15)
016CR     15   FORMAT (////, 5X, 'Q/N' , 21X, 'HSP', 17X, 'CHECK', 23X,'PERCENT')
01A6R     C
01A6R          TOTERR = 0.
01AER     C
01AER          DO 10 J = 1, ND
01B6R          CHECK(J) = COEFF(1) + COEFF(2)*FLCOFF(J) + COEFF(3)
01B6R         1 *FLCOEF(J)**2 + COEFF(4) * FLCOEF(J)**3 + COEFF(5)*FLCOEF(J)
01B6R         2 **4 + COEFF(6)*FLCOEF(J)**5 + COEFF(7) * FLCOFF(J)**6
02CAR          PLOT (3,J) = CHECK(J)
02FCR          PERCEN(J) = CHECK(J) / HSP(J)
0338R          ERR = 1.- ABS (PERCEN(J))
0364R          TOTERR = TOTERR + ERR
0370R          WRITE (5,20) FLCOEF(J), HSP(J), CHECK(J), PERCEN(J),ERR
040CR     20   FORMAT (/, E13.5, 10X, E13.5, 10X, E13.5, 20X,F10.4, 15X,F10.4)
0444R     10   CONTINUE
0454R     C
0454R          AVERR = TOTERR/AND
0460R          WRITE (5,25) TOTERR, AVERR
0484R     25   FORMAT (////, '     THE TOTAL ERROR IS    ',F10.4,'    AND THE  AVG.
0484R         1 ERROR IS     ', F10.4)
04DAR           CALL QPICTR (PLOT, 3, 29, QY(2,3), QX(1), QLABEL(-1103))
051ER           PAUSE
0524R          CALL QPICTR (PLOT,3,29, QY(2), QX(1), QLABEL(-1103))
0566R          PAUSE
056CR          CALL QPICTR (PLOT,3, 29, QY(3), QX(1), QLABEL(-1103))
05AER          PAUSE
05B4R          END
```

SINGLE-PHASE DATA CURVE-FIT (continued)

```
0004R            SUBROUTINE LSFIT(NPTS, NPARAM, X, Y, PARAM)
0034R      C
0034R            REAL X, Y, PARAM, A, XPOWER, XP, XK, YK
0034R            INTEGER NPTS, NPARAM, I, K, IXPMAX, IERR
0034R      C
0034R            DIMENSION X(NPTS), Y(NPTS), PARAM(NPARAM)
0034R      C
0034R      C  TO USE A VALUE OF NPARAM GREATER THAN 10, THE USER SHOULD CHANGE
0034R      C  THE LENGTH OF A TO AT LEAST NPARAM**2, AND THE LENGTH OF XPOWER
0034R      C  TO AT LEAST 2*(NPARAM-1).
0034R            DIMENSION A(100), XPOWER(18)
0034R      C
0034R      C  CHECK FOR ARGUMENT ERRORS.
0034R            IF (NPTS .GE. NPARAM .AND. NPARAM .GT. 0) GO TO 10
0060R            WRITE (5, 1001) NPTS, NPARAM
009CR            RETURN
00A4R      C
00A4R      C  ZERO ARRAYS BEFORE SUMMING.
00A4R         10 DO 20 I = 1, NPARAM
00ACR         20    PARAM(I) = 0.0E0
00E2R      C
00E2R            IXPMAX = MAX0(1, 2 * (NPARAM - 1))
0106R            DO 30 I = 1, IXPMAX
010ER         30    XPOWER(I) = 0.0E0
0136R      C
0136R      C  COMPUTE SUMS OF POWERS OF X AND OF POWERS OF X TIMES Y.
0136R            DO 50 K = 1, NPTS
013ER               XP = 1.0E0
0146R               XK = X(K)
0168R               YK = Y(K)
018AR               DO 40 I = 1, IXPMAX
0192R                  IF (I .LE. NPARAM) PARAM(I) = PARAM(I) + XP * YK
01E8R                  XP = XP * XK
01F4R                  XPOWER(I) = XPOWER(I) + XP
0220R         40    CONTINUE
0230R         50 CONTINUE
```

SINGLE-PHASE DATA CURVE-FIT (continued)

```
0244R   C
0244R   C  COMPUTE COEFFICIENTS OF NORMAL EQUATIONS.  THE COEFFICIENT MATRIX
0244R   C  HAS A BANDED STRUCTURE.
0244R         A(1) = NPTS
025AR         IF (NPARAM .EQ. 1) GO TO 90
0270R   C
0270R         DO 80 I = 2, NPARAM
0278R            XP = XPOWER(I - 1)
0296R            DO 60 K = 1, I
029ER   C
029ER   C            A(K, I + 1 - K) = XP
029ER         JK=(K+NPARAM *(I-K))
02B6R         A(JK) = XP
02CER      60    CONTINUE
02DER   C
02DER         JL =(NPARAM + I -2)
02F2R         XP = XPOWER (JL)
030AR            DO 70 K = I, NPARAM
0312R   C
0312R   C            A(NPARAM + I - K, K) = XP
0312R         JH =(I + (NPARAM -1 ) * K)
032AR         A(JH) = XP
0342R      70    CONTINUE
0356R      80 CONTINUE
036AR   C
036AR   C  SOLVE NORMAL EQUATIONS.
036AR      90 CALL SIMQ(A, PARAM, NPARAM, IERR)
0390R         IF (IERR .NE. 0) WRITE (5, 1002)
03B2R         RETURN
03BAR   C
03BAR    1001 FORMAT(23H LSFIT:  ARGUMENT ERROR, 2I11)
03E2R    1002 FORMAT(39H LSFIT:  NORMAL EQUATIONS ARE SINGULAR.)
0414R         END
```

CALCULATION OF ψ'_{tpth} FOR THE PLASTIC IMPELLER DATA

```
0004R          DIMENSION NUM(100), QTOT(100), N(100), PRESS(100), VOID(100)
0004R         DIMENSION SLIP(100), DENAIR(100), A(100), PHI(100), HTHTP(100)
0004R         DIMENSION QAIR(100), QWAT(100)
0004R    C
0004R          AREA = 0.25*28. /144.
0014R         AA = 1.0
001CR         ND=91
0024R         B=-1.1200114
0030R         CF=671.75
0038R    C
0038R         WRITE (5,8)
004CR     8   FORMAT(1H1, //,30X,'CALCULAING THE TWO-PHASE FLOW FUNCTION OF THE
004CR        1RUBBER PUMP.')
009CR    C
009CR         WRITE(5,9)
00B0R     9    FORMAT(///,4X, 'TEST NO.', '  TOTAL FLOW', 5X, 'SPEED',12X,
00B0R        1'VOID', 12X,'SLIP',5X,'SUPERFICIAL', 5X,'SUPERFICIAL',4X,
00B0R        2'TWO-PHASE',3X,' THEORETICAL')
013CR    C
013CR         WRITE (5,10)
0150R     10  FORMAT(15X,'CU.FT/SEC', 7X,'RPM',3X,'FRACTION',11X,'RATIO',5X,
0150R        1 'VEL AIR',9X,'VEL LIQ',10X,'FUNCTION',2X,'TWO-PHASE HEAD')
01C8R    C
01C8R         DO 5 I = 1, ND
01D0R         READ(8,6) NUM(I), QWAT(I), QAIR(I), N(I), PRESS(I), VOID(I)
02A4R     6   FORMAT (I10, 2F12.5, I10, 2F12.4)
02C2R    C
02C2R    C    CALCULATE THE DENSITIES OF WATER AND AIR.
02C2R         DENWAT = 62.4
02CAR         DENAIR(I) = (PRESS(I) + 14.7) *144. / (53.34*530.)
030ER    C
030ER         AIRMAS= QAIR(I) * DENAIR(I)
033AR         WATMAS = QWAT(I) *  DENWAT
0356R         TOTMAS= AIRMAS + WATMAS
0362R         X = AIRMAS / TOTMAS
036ER         QTOT(I) = QAIR(I) +QWAT(I)
03AAR         SPAIR = TOTMAS * X / (DENAIR (I) * AREA)
03DAR         SPWAT = TOTMAS * (1.-X) / (DENWAT * AREA)
03FER         SLIP(I) = SPAIR * (1.-VOID(I)) /(SPWAT * VOID(I))
0452R         A(I) = (VOID(I) /(1.-VOID(I))) * DENAIR(I)/ DENWAT
04AER         PHI(I) = (1.+A(I)) * (1.+ SLIP(I)**2 * A(I))/( 1. + SLIP(I)*A(I))
04AER        1 **2
0556R         HTHTP(I) = AA + B* PHI(I) * (QTOT(I) / (FLOAT(N(I))))*CF
05CAR    C
05CAR         WRITE (5,7) NUM(I) ,QTOT(I),N(I),VOID(I),SLIP(I),SPAIR,
05CAR        1 SPWAT, PHI(I), HTHTP(I)
05CER      7  FORMAT (/,4X, I4,6X, F10.5, I10,4X, 6(F12.5,3X))
06FAR     5   CONTINUE
070AR          END
```

CALCULATION OF H* FOR THE BRONZE IMPELLER DATA

```
0004R          DIMENSION PLOT(7,51)
0004R          DIMENSION PLOT2 (5,51)
0004R          DIMENSION XSCL (4)
0004R          DATA XSCL /0.0, 0.50, 0., 3.0/
0018R     C
0018R          DO 11 II = 1,5
0020R          DO 12 JJ = 1,51
0023R          PLOT2 (II,JJ) = 0.072
004AR     12    CONTINUE
005AR     11   CONTINUE
006AR          AA = 1.0
0072R          AREA = 0.0581
007AR          ND=51
0082R          B= -4.511
008ER          CF1 = 539.44
0096R          CF2 = 2635.774
009ER          ISCL = -2
00AAR     C
00AAR          WRITE (5,23)
00BER     23   FORMAT(1H1, 3X,'TEST NO.', 2X, 'VOID FRACTION', 5X,
00BER         1'FLOW COEFF', 5X, 'HTHTP', 12X, 'HTP', 10X, 'HTHSP',
00BER         2 12X, 'HSP', 13X,'RATIO')
0132R     C
0132R          DO 5 I = 1, ND
013AR          READ (8,6) NUM, QWAT, QAIR, N, PRESS, VOID , DELH
0186R      6   FORMAT (I10, 2F12.5, I10, 3F12.5)
01A4R          DENWAT = 62.4
01ACR          DENAIR = (PRESS +14.7) *144. /(53.34 * 530.)
01D0R          QTOT= QAIR + QWAT
01DCR     C
01DCR          SPAIR = QAIR/ AREA
01E8R          SPWAT = QWAT / AREA
01F4R          SLIP = SPAIR *(1. - VOID) / (SPWAT* VOID)
0218R          A= (VOID/ 1. - VOID) * DENAIR / DENWAT
0230R          PHI = (1.+A)*(1.+SLIP**2*A)/(1.+SLIP*A)**2
0278R          FLCEF= (QTOT/FLOAT(N)) *CF1
0290R     C
0290R          HTHTP = AA+ B*PHI *(QTOT/FLOAT(N)) *CF1
02BCR          HTHSP = AA+ B*(QTOT/FLOAT(N)) *CF1
02DCR          HSP = .41315 + .57951*FLCEF - 5.7719*FLCEF**2- 614.27*FLCEF**3 +
02DCR         17931.1*FLCEF**4 -48526.*FLCEF**5 +106810.*FLCEF**6
0370R          HTP= (DELH /FLOAT(N) **2) *CF2
0390R          RATIO = (HTHTP-HTP)/(HTHSP-HSP)
03B0R     C
03B0R          PLOT (1,I) = FLCEF
03D2R          PLOT (2,I) = HTHTP
03F4R          PLOT(3,I) = HTP
0416R          PLOT(4,I) = HTHSP
0438R          PLOT(5,I)= HSP
045AR          PLOT(6,I) = RATIO
047CR          PLOT(7,I) = VOID
049ER          IF(FLCEF.LE.0.08) PLOT2(1,I)=RATIO
04CER          IF(FLCEF.GT.0.08.AND.FLCEF.LE.0.11) PLOT2(2,I)=RATIO
```

CALCULATION OF H* FOR THE BRONZE IMPELLER DATA (continued)

```
050CR           IF(FLCEF.GT.0.11.AND.FLCEF.LE.0.14) PLOT2(3,I)=RATIO
054AR           IF(FLCEF.GT.0.14) PLOT2(4,I)= RATIO
057AR           PLOT2(5,I)=VOID
059CR     C
059CR            WRITE (5,18) NUM, VOID, FLCEF,HTHTP, HTP, HTHSP, HSP, RATIO
05FOR      18   FORMAT (3X, I10, 7(F10.5,5X),/)
060CR      5    CONTINUE
061CR           CALL QPICTR (PLOT, 7, ND, QY(2,3,4,5), QX(1), QLABEL(-1003))
0664R           PAUSE
066AR     C
066AR           CALL QPICTR (PLOT2,5,ND, QY(1), QX(5), QLABEL(-1003),
066AR          1QISCL(-2),QXSCL(XSCL))
06D4R           PAUSE
06DAR           CALL QPICTR (PLOT2,5,ND, QY(2), QX(5), QLABEL(-1003),
06DAR          1QISCL(-2),QXSCL(XSCL))
0744R           PAUSE
074AR           CALL QPICTR (PLOT2,5,ND, QY(3), QX(5), QLABEL(-1003),
074AR          1QISCL(-2),QXSCL(XSCL))
07B4R           PAUSE
07BAR           CALL QPICTR (PLOT2,5,ND, QY(4), QX(5), QLABEL(-1003),
07BAR          1QISCL(-2),QXSCL(XSCL))
0824R           PAUSE
082AR           END
```

REFERENCES

2-1 Wilson, David Gordon, private communication, January 13, 1976.

2-2 Dixon, S. L., FLUID MECHANICS, THERMODYNAMICS OF TURBOMACHINERY, 2nd edition, Pergamon Press, Oxford, U.K., 1975, pp. 196-203.

2-3 Bean, Howard S., ed., FLUID METERS, THEIR THEORY AND APPLICATION, 6th edition, A.S.M.E., N.Y., 1971.

3-1 Chan, T. C., CURVE-FITTED DATA, COMPUTER PROGRAM, M.I.T., December 6, 1976.

3-2 Collier, J. G., CONVECTIVE BOILING AND CONDENSATION, McGraw-Hill, London, 1972, pp. 65-82.

3-3 Griffith, Peter, private communication, July 7, 1976.

3-4 Olson, D. J., SINGLE- AND TWO-PHASE PERFORMANCE CHARACTERISTICS OF THE MOD-1 SEMISCALE PUMP UNDER STEADY-STATE AND TRANSIENT CONDITIONS, Aerojet Nuclear Company, ANCR Report 1165, October, 1974, pg. 61.

4-1 Wilson, D. G., Chan, T. C., Goldfinch, A. L. and Zegley, R. D., ANALYTICAL MODELS AND EXPERIMENTAL INVESTIGATION OF CENTRIFUGAL PUMP PERFORMANCE IN TWO-PHASE FLOW, EPRI Final Report RP 493-1, M.I.T., December, 1976.

4-2 Mikielewicz, J., Wilson, D. G., Chan, T. C., Goldfinch, A. L., A METHOD FOR CORRELATING THE CHARACTERISTICS OF CENTRIFUGAL PUMPS IN TWO-PHASE FLOW, ASME paper 76-WA/FE-29, N.Y., August 12, 1976, pp. 3-5.

7-1 Nilsson, K. A., THIRD MEETING NOTES, EPRI Performance Review Group, Palo Alto, CA, October 7, 1976, pg. 3.

A-1 Csanady, G. T., HEAD CORRECTION FACTORS FOR RADIAL IMPELLERS, Engineering, London, 1960, pg. 190.